2011

Biophysical Characterization of the Membrane Binding Domain of the Pro-apoptotic Protein Bax

Pranav Garg
University of Central Florida

BIOPHYSICAL CHARACTERIZATION OF THE MEMBRANE BINDING DOMAIN OF THE PRO-APOPTOTIC PROTEIN *BAX*

by

PRANAV GARG
B.Tech. (Biotechnology)
Amity University, Noida, India, 2009

A thesis submitted in partial fulfillment of the requirements
for the degree of Masters in Science
in the Department of Biotechnology
in the Burnett School of Biomedical Sciences, College of Medicine
at the University of Central Florida
Orlando, Florida

Summer Term

2011

Major Professor: Suren A. Tatulian, PhD

ABSTRACT

The BCL-2 family of proteins tightly regulates the delicate balance between life and death. The pore forming Bax is a pro-apoptotic member belonging to this protein family. At the onset of apoptosis, monomeric cytoplasmic Bax translocates to the outer mitochondrial membrane, forms oligomeric pores thereby letting mitochondrial cytochrome *c* enter the cytosol and initiate the apoptotic cascade. The C-terminal "helix 9" is thought to mediate the membrane binding of BAX. A 20-amino acid peptide corresponding to Bax C-terminus (VTIFVAGVLTASLTIWKKMG) and two mutants where the two lysines are replaced with Glu (charge reversal mutant, EE) or Leu (charge neutralization mutant, LL) have been studied to elucidate the pore formation capabilities of Bax C-terminus and the underlying molecular mechanism. Interactions of the wild-type and the two mutant peptides with zwitterionic and anionic phospholipid membranes caused efficient membrane permeabilization, as documented by release of vesicle-entrapped fluorescent indicator calcein. Light scattering experiments showed that vesicles maintained their integrity upon peptide binding, indicating that the content leakage was due to pore formation and not vesicle degradation. Kinetics of calcein release at various peptide concentrations were used to determine the peptide-peptide association constants and the oligomeric state of the pore.

The structure of membrane-bound peptides was analyzed by circular dichroism (CD) and attenuated total reflection-Fourier transform infrared (ATR-FTIR) spectroscopy. CD data indicated all three peptides reconstituted in lipid vesicles contained α-helical and β-strand structures. ATR-FTIR experiments indicated that the minimally hydrated samples of peptides in stacked lipid bilayers (absence of bulk water) were mostly α-helical but adopted mostly β-sheet

conformation in the presence of excess water.

Finally, the depth of membrane insertion of the peptides was analyzed using tryptophan fluorescence quenching by dibromo-phosphatidylcholines brominated at various positions of their acyl chains. In case of zwitterionc phospholipid membranes, the single Trp^{16} was located at ~9 Å from membrane center. In case of membranes containing 30% of an anionic phospholipid, the depth of membrane insertion of the EE mutant was not affected but the wild-type and the LL mutant peptides were embedded much deeper into the membrane, with Trp^{16} located at 3-4 Å from membrane center.

These results will help achieve a better understanding of the molecular mechanism of membrane pore formation of Bax protein. In addition, they provide insight into the molecular details of membrane pore formation by peptides and could facilitate the design and production of cytotoxic peptides with improved capabilities to lyse cells such as bacteria or cancer cells.

Karmanye vadhikaraste ma phaleshu kadachna
Karmaphalehtur bhurma te sangostvakarmani.
Ch. 2, 4- Sreemad Bhagwadgeeta.

"You have a right to perform your prescribed duty, but you are not entitled to the fruits of action. Never consider yourself the cause of the results of your activities, and never be attached to not doing your duty."

This thesis is dedicated to my Parents, who against all odds have sent me to the United States to pursue this dream….

ACKNOWLEDGMENTS

My words would not be enough to express gratitude to my supervisor, mentor and committee chair, Dr. Suren A. Tatulian, for his direction, assistance, and guidance. In particular his recommendations and suggestions have been invaluable for the project. I would also like to acknowledge the support of my esteemed committee members Dr. Annette Khaled, Dr. Saleh Naser and also Biotechnology Graduate Program coordinator Dr. Henry Daniell.

I also wish to thank our very dear Research Associate Dr. Kathleen N. Nemec who taught me several techniques and sailed me through the difficult times of my project.

Special thanks should be given to my colleague and dear friend, Supriyo Ray who helped me in many ways and for being such a great lab mate. Finally, words alone cannot express the thanks I owe to God to giving me a chance to study the Science and contribute to the development of the world.

My stay in the beautiful state of Florida has been delightful because of friends and my near and dear ones. My parents and siblings for standing by me and motivating me every time I would feel depressed during this journey called Education. With the Grace of God; I hope to continue and succeed in the MBA program in College of Business Administration at this beautiful University of Central Florida.

Thank you all for being a part of my life.

TABLE OF CONTENTS

LIST OF FIGURES

LIST OF TABLES

CHAPTER 1. INTRODUCTION

1.1 Apoptosis

Nature has an on-going balanced phenomenon called Apoptosis, which primarily is the key player in controlling several important processes in the body including maintenance of tissue homeostasis and normal development. Apoptosis, also called programmed cell death participates in homeostasis and removes any defective cells (Mancinelli, Caraglia, Budillon, Abbruzzese, & Bismuto, 2006) and is a highly regulated process involving several different pathways and millions of proteins working in perfect coordination.

The mechanism that dictates apoptosis is highly complex. As we mentioned, it consists of a large number of proteins which in turn participate in several mechanisms for signaling, commitment and execution of apoptosis via numerous simultaneous pathways (Yu & Zhang, 2004). So when a cell is committed to die, it attains very distinct phenotypic characteristics, such as blebbing, destruction of nuclear material by condensation of chromatin. The end result is many small apoptotic bodies that can be engulfed by macrophages. All this is to ensure that only the cell in which apoptotic stimulus is generated is affected and all other cells in the vicinity are protected. In case if there is a malfunctioning in the apoptotic machinery, the result can be disastrous, such as uncontrolled cell growth found in many diseases. These defective cells survive to collect further mutations and can even grow under hypoxia and oxidative stress. Conversely, in several neurodegenerative diseases such as Huntington's, Parkinson’s or Alzheimer's disease, there has been shown death of selective neurons which can result in loss of memory and involuntary

muscle movements. There are two commonly observed pathways which induce cell death signals leading to Apoptosis: extrinsic or intrinsic. The extrinsic pathway is initiated by the formation of death-inducing signaling complex (DISC), and intrinsic pathway where an internal signal activates Bax, which then translocates to the mitochondria, releasing cytochrome c, propagating the caspase cascade (Ashkenazi, 2002).

1.2 BC_L Associated X-protein

Bax is a member of the BCL-2 family. The BCL-2 family members are known to be pro and anti-apoptotic proteins which participate in various cell functions. During the apoptotic signal, Bax inserts itself on the outer mitochondrial membrane, causing membrane destruction and permeabilization. This results in release of the contents from the inside of the mitochondria into the cytosol. Several studies have been performed where Bax structure and its sub cellular location were determined. Cytochrome c associates with Apaf-1 and Procaspase 9 forming apoptosome, which in turn degrades all internal proteins (Gogvadze, Orrenius, & Zhivotovsky, 2006). All this happens by an antagonistic relationship between the pro and anti-apoptotic proteins in the Bcl-2 family.

As far as the structural similarities go in various Bcl-2 family members, it has been found that each member has one or more 'Bcl-2 Homology' regions. Bax contains 9 α-helices and 3 out of the four of the BH regions (Reed, 2006). The NMR structure of Bax shows two hydrophobic α-helices hidden from the aqueous phase by seven amphipathic α-helices (Suzuki et. al, 2000). A hydrophobic cleft can be found that is thought to be where the BH3 domains of the Bax and Bak

interact (Veresov & Davidovskii, 2009). The Three dimensional backbone structures of Bax, BCL-2 and BCL-xL can be superimposed on each other (Suzuki, Youle, & Tjandra, 2000). It is only the α9 helix that sits in the hydrophobic pocket and participates in the heterodimer formation with its antagonist. Because of the apparent significance of Bax's C-terminal α9-helix, this project deals with studying its structure and function, i.e., elucidation of pore forming capabilities and the underlying molecular mechanism.

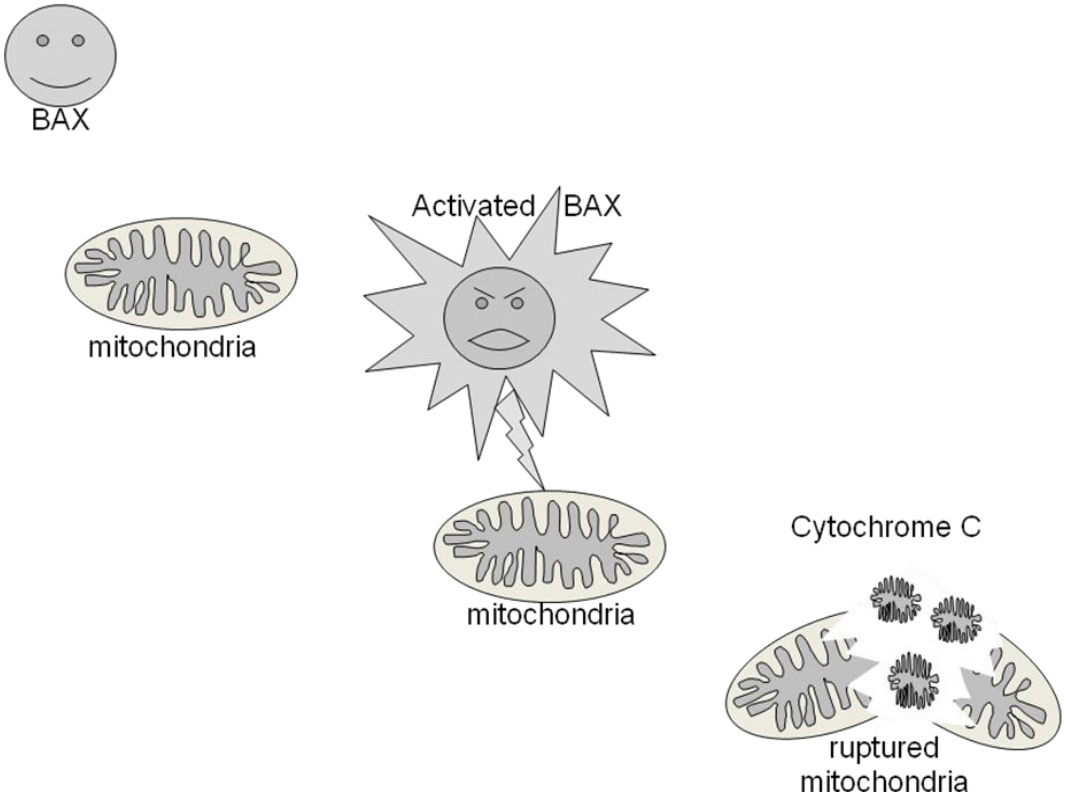

Figure 1: Process of Apoptosis happening inside the Cell affecting the power house of the cell- Mitochondria.

Lipid vesicles were used to model the interaction of Bax C-terminal α-helix with membranes (Kuwana et al., 2002). Additionally, Bak, another pro-apoptotic BCL-2 family member was shown to have its secondary structure modified by the composition of lipid membrane. But it is still unknown whether the α9 helix acts as a protein anchor or is itself a participant in pore formation.

The focus of this project was on demonstration that the C-terminal α-9 helix of Bax-C, when isolated from the protein as an individual peptide, can form pores in lipid membranes, and identification of the biophysical characteristics of the pore, such as the peptide structure, peptide-peptide affinities within the membrane, and the oligomeric state of the pore.

We used circular dichroism (CD), Fourier transform infrared (FTIR) spectroscopy and fluorescence methods to determine the mode of interaction of Bax-C with membranes and pore formation. The effect of membrane electrostatics on peptide-membrane interactions was probed by using zwitterionic membranes composed of 100% 1-palmitoyl-2-oleoyl-*sn*-glycero-3-phosphocholine (POPC), and membranes composed of 70% POPC and 30% of an anionic lipid 1-palmitoyl-2-oleoyl-*sn*-glycero-3-phosphoglycerol (POPG). To probe the importance of the double lysine residues near the C-terminus of the α-9 helix of Bax, in parallel to the wild-type peptide two mutants have been studied where the two lysines were replaced with Glu (charge reversal mutant, EE) or Leu (charge neutralization mutant, LL).

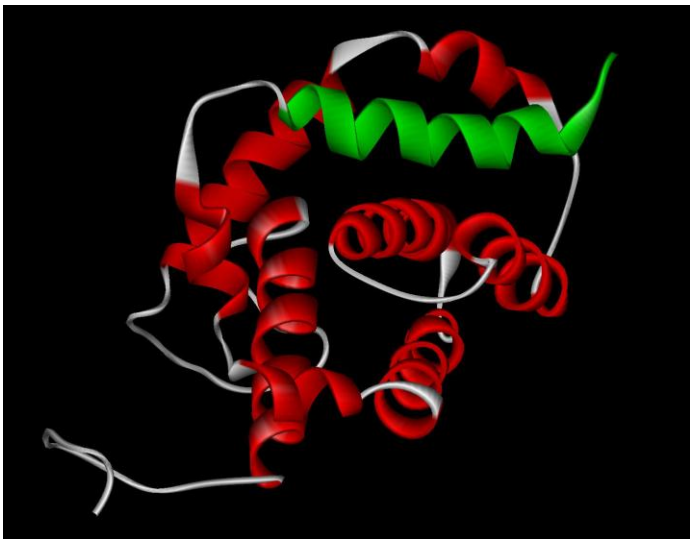

Figure 2: The NMR structure of BAX (Suzuki et al., 2000). Helices are colored red, and the C-terminal helix 9 is highlighted in green.

1.3 Bax Oligomerization and Localization

Based on previous studies, we have tested the *working hypothesis* that key mitochondrial targeting elements reside in Bax's C-terminus. We have examined a putative membrane- binding stretch of Bax, i.e., the C-terminal helix that contains double lysines at positions 189 and 190 (Petros, Olejniczak, & Fesik, 2004; Reed, 2006). The same biophysical techniques like FTIR and CD were used to define the parameters of membrane insertion using synthetic membranes in the form of large unilamellar vesicles (LUVs).

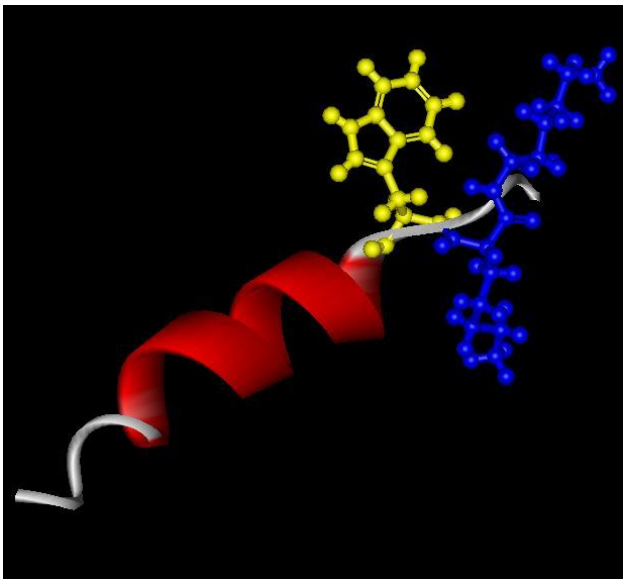

Figure 3: C-terminal helix 9 of Bax is shown with residues Trp 16 and Lys 17, 18 highlighted in yellow and blue, respectively (Suzuki et al., 2000).

1.4 Objective of the project

The main objective of this project was to test the hypothesis that the α-9 helix of Bax has membrane binding and pore forming capability and identify the molecular and structural basis of pore formation. Vesicle content leakage and biophysical studies have been carried out using synthetic peptide with the sequence (VTIFVAGVLTASLTIWKKMG), which corresponds to the last 20 amino acids of Bax to accomplish this objective. The contribution of the two lysine residues to the structure and membrane permeabilization activity of the peptide was studied by using two mutants of the synthetic 20-mer peptide where the lysines were replaced with either glutamic acid or leucine residues. The effect of membrane charge was evaluated by using

zwitterionic POPC membranes as well as membranes containing 70% POPC and 30% of an anionic lipid POPG. These studies were aimed at achieving a molecular model of the membrane pores made by the Bax C-terminal peptide, which would have a two-fold impact. First, identification of the mode of membrane binding and membrane permeabilization by the peptide would provide molecular insight into the mechanism of action of Bax on mitochondrial membranes. Second, analysis of the structure and pore forming activities of the wild-type and mutant peptides would open new possibilities for design and production of potential cytotoxic peptides that could kill bacteria, fungi, or cancer cells by perforation of their plasma membranes.

CHAPTER 2. LITERATURE REVIEW

2.1 Are there Bax receptors in OMM?

With the induction of apoptotic stimuli, Bax translocates to the Outer Mitochondrial Membrane (OMM) from the cytosolic environment with the aim of permeabilizing OMM. Due to this, all other cellular structures maintain their integrity at the beginning of apoptosis and only Bax functions at this time. If this is not true, then the cell would become necrotic leading to complete disassociation of the entire cellular environment. Hence, the reason for Bax to go first and bind specifically to the OMM is because of the type of lipids along with membrane bound proteins which can be classified as either membrane bound proteins with a single or multiple α-helical transmembrane domains or proteins with predominant β-structure (Ott, Norberg, Zhivotovsky, & Orrenius, 2009). Bax falls in the first category and carries a positive charge with an isoelectric point of 10.5, facing the intermembrane space, which is a characteristic of several other single membrane spanning proteins (Martínez-Senac, Corbalán-García, & Gómez-Fernández, 2002).

OMM has a distinct lipid composition, in that cardiolipin is present in mitochondrial membranes at significant quantities. Cardiolipin binds cytochrome c, which is found in the mitochindrial matrix. This interaction controls the degree of cytochrome c demonstrating that apoptosis is a highly regulated phenomenon. It has also been shown that cardiolipin is a receptor for Procaspase 8, another apoptotic regulator (Garcia-Saez, Fuertes, Suckale, & Salgado, 2010; Gogvadze et al., 2006; Lovell et al., 2008). Strong evidences have been provided for mitochondrial targeting of tBid and Bax to the outer membrane of other cellular organelles.

However there is a very little cardiolipin (roughly 0.3-1.4%) found in the OMM but often researchers are using 10-40% of cardiolipin which strongly exceeds the amount in OMM to answer the questions about the presence of receptors. An integral protein of OMM- VDAC, forms complexes BCL-2 family proteins Bax, Bak, and tBid and is considered as a "receptor" for these proteins (Zeth et al, 2010). However, no strong evidence has yet been provided for the existence of specific Bax receptors.

2.2 Knowledge about Bax structure and function

2.2.1 Current knowledge about Bax

Even though several studies have shown that mitochondrial translocation of Bax causes the up regulation of Ca^{2+}stores with its association with pro-apoptotic proteins, the accurate mechanism of Bax is still unknown (Zong et al., 2003). Out of the several studies performed on Bax over the years, one suggests that Bax permeabilization of the OMM is due to the similarity in structure between the multi domains of BCL-2 family with diphtheria toxin, which forms protein-translocating pores in the endosomal membrane (Yip & Reed, 2008). Another study suggests that upon Bax binding, fragmentation of mitochondria takes place (Karbowski & Youle, 2003). Even with these studies, the molecular determinants of binding of Bax to the mitochondrial membrane, the pore structure and its oligomeric state remain elusive. Protein-protein interactions have been experimentally studied to elucidate the translocation mechanism and its mode of action. A very commonly used assay system, called Yeast two-hybrid system was established (Willis et al.,

2005). It is thought that Bax self associates through BH_1 and BH_2 domains. If there is any anomaly in the heterodimers, then the cell becomes more susceptible to apoptosis.

Apart from BLC-2 family of proteins, several other signaling pathway proteins also contibute to the regulation of Bax. Important among those is a serine threonine kinase called AKT which inhibits structural change within Bax, which may inhibit mitochindrial binding, preventing apoptosis (Brunet et al., 1999). Since no regulatory changes have been observed in the Bax phosphorylation, the mechanism of AKT inhibition is still not clear. In human keratinocytes, on the other hand, UVB activation of p38 MAP Kinase promotes the movement of Bax to mitochondria. Several upstream effector proteins also modulate the activity of Bax but even with these theories, the actual mechanism for the membrane translocation is still unclear (Reed, 2006; Torrecillas et al., 2005).

2.2.2 Gap in knowledge about Bax

While previous research in the BAX field has given enormous information about the regulation and mechanism of BAX, the key players in its activation have not been identified. Even the recent structural studies are somewhat contradictory and do not reveal the mechanism of Bax activation. One study suggests that the C-terminal domain is the major component in the protein responsible for membrane insertion while the other study proposed that the amino terminal acts a mitochondrial targeting sequence (Karbowski & Youle, 2003; Zong et al., 2003).Yet another study comes across as a contradictory to the two previous studies and suggests that the pivotal role of the N-terminal domain is the commitment to apoptosis (Gogvadze et al, 2006). The role of Bax α-9 helix segment has also been suggested as a transmembrane domain that could

translocate BAX to the OMM (Ausili et al. 2008). So due to these ambiguous results, there is a strong need to gather well defined structural data which focuses on the mechanism of activation and function of Bax with respect to the lipid membrane binding. In order to fill this gap, more work needs to be performed to determine the critical membrane binding domains in the BAX structure and also its intermolecular and intra molecular interactions (Tschammer, 2007).

2.3 Analysis of Protein−Lipid Systems by ATR-FTIR Spectroscopy

In an attenuated total reflection- Fourier transformed infrared (ATR-FTIR) experiments, an internal reflection plate made of high quality Germanium is used to deposit the peptide on its surface (Tatulian et al., 1995). A thin layer of lipid containing the reconstituted peptide is deposited and an infrared beam is directed onto the plate. The beam undergoes several internal reflections from one end of the plate to another, leading to an exponentially decaying evanescent field at both surfaces of the Ge plate. Because energy is transferred from the evanescent field to the deposited layer of lipid and peptide, a distinct absorption spectrum will be generated which carries a plethora of structural information for both the lipid and protein (of peptide) molecules. FTIR spectroscopy is very sensitive to protein conformational changes and is not limited to the molecular size of the sample (Jackson & Mantsch, 1995). Another advantage of using ATR-FTIR for peptide structure determination is due to absence of light scattering problems unlike circular dichroism or fluorescence experiments in the UV region. ATR-FTIR is unique in that the spectrum of any protein-lipid combination does not require any labeling and generates well-

resolved absorbance bands for both lipids and proteins and also for various structural groups of these protein molecules (Goormaghtigh et al., 1990; Tatulian et al., 1995).

Secondary structure of proteins can be elucidated by amide I absorption frequencies which is generated by the contributions from the C=O (80%) and C-N vibrational stretching found between 1600 to 1700 cm^{-1}. The particular characteristics of the structural components that make up the amide I mode can be used to calculate the proportion of a protein's secondary structure (different secondary structures generate amide I vibration at distinct frequencies) (Tamm & Tatulian, 1993). N-H bending (60%) and C-N stretching (40%) contribute to the amide II band, and is found between 1520 to 1580 cm^{-1}. It is perhaps the most useful spectral range in measuring the amide H/D exchange and the protein's "dynamic structure".

Table 1: Amide I Frequencies of Most Typical Secondary Structural Elements in Proteins in H_2O and D_2O Environments (Tatulian, 2003).

	frequency(cm^{-1})	
Secondary structure	**H_2O**	**D_2O**
α_I-helix	1658−1650	1655−1646
α_{II}-helix	1666−1658	1658−1652
3_{10}-helix	1670−1660	1670−1660
↑↓β-sheet	1638−1632	1636−1630
↑↓β-sheet	1695−1675	1680−1670
Intermolecular β-sheet	1625−1615	1625−1615
β-turns	1685−1655	1675−1640
γ-turns	1690−1650	1690−1650
irregular	1660−1652	1648−1640
Amide or aromatic side chains	1618−1605	1615−1600

2.4 Lipid Monolayers and Bilayers

Several models have been established to study the cellular membranes which will mimic the natural environment inside the cell (Liu & Regen, 1993). For this purpose, lipid vesicles have been used as model membranes which will allow the study of protein interaction with the

mitochondrial membrane (Frey & Tamm, 1991). One very commonly used method for deposition of lipid on the solid surface would be direct spreading but this method has the limitation since not all the protein can be uniformly distributed across the area of the Ge plate. Other than that the dry protein-lipid solution is believed to be far from the physiological state of the actual cellular environment (Fa et al., 2006). Real physiological condition can be modeled to a greater amount in comparison to the systems where dried lipid samples are deposited.

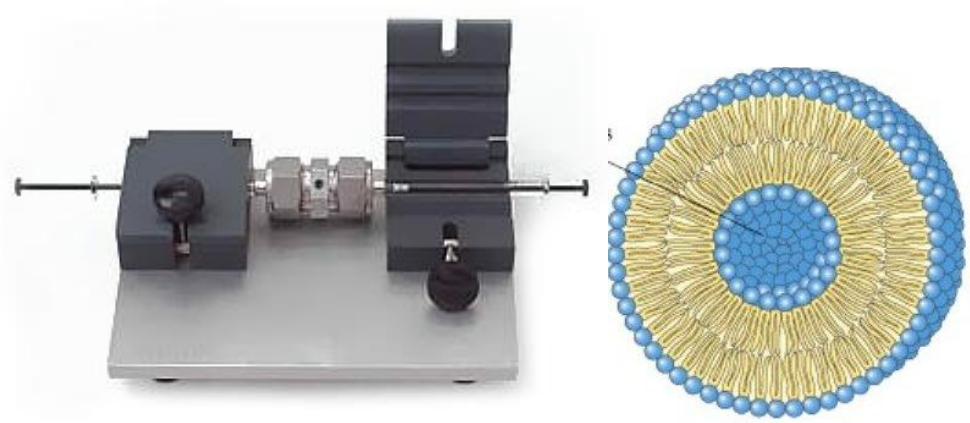

Figure 4: Creating of Large Unilameller Vesicles using extruder (left) and POPC LUV is created by passing through 100 nm pore size membrane 15-20 times (right). (Courtesy Avanti Polar Lipids, Alabaster, AL)

Langmuir-Blodgett (LB) technique is used to deposit the lipid monolayer on the Ge plate. In order to create a lipid bilayer, lipid vesicles containing peptide are injected into the ATR cells so that the peptide-lipid vesicle suspension gets deposited on top of the already coated monolayer. The vesicles have been prepared by sonication and are 30-50 nm in diameter. Once the bilayer is

created, secondary structure can be determined using spectral measurements obtained at two different polarizations of the incident light (Jackson, Haris, & Chapman, 1989).

2.5 Circular Dichroism (CD)

We used Circular Dichroism (CD), a well known method for protein secondary structure determination (Brenner et. al, 2000) as a complementary method to FTIR. The asymmetry of the α-carbon backbones of proteins result in chirality leading to optical activity. This optical activity can be useful for the study of α helices or β-sheets which constitute large fractions of most proteins. Secondary structure determination from CD is done using a number of modeling techniques.

CD spectra are composed of the difference in the absorption of plane polarized light, which has been resolved into its left and right handed components. The following equation is used:

$$\Delta\varepsilon = \varepsilon_L - \varepsilon_R$$

Where ε is the molar extinction coefficient for either the left (L) or right (R) vectors, respectively. The emerging beam is elliptically polarized (Fu et al., 1998). CD spectrum for each type of secondary structure is different and hence is a characteristic feature of each secondary structure. The spectrum for an α helix has two minima at 208 nm and 222 nm, β- sheets only give one minima at 215 nm. The spectrum of unordered structures has a weak maximum around 220 nm along with a deep minimum at 200 nm.

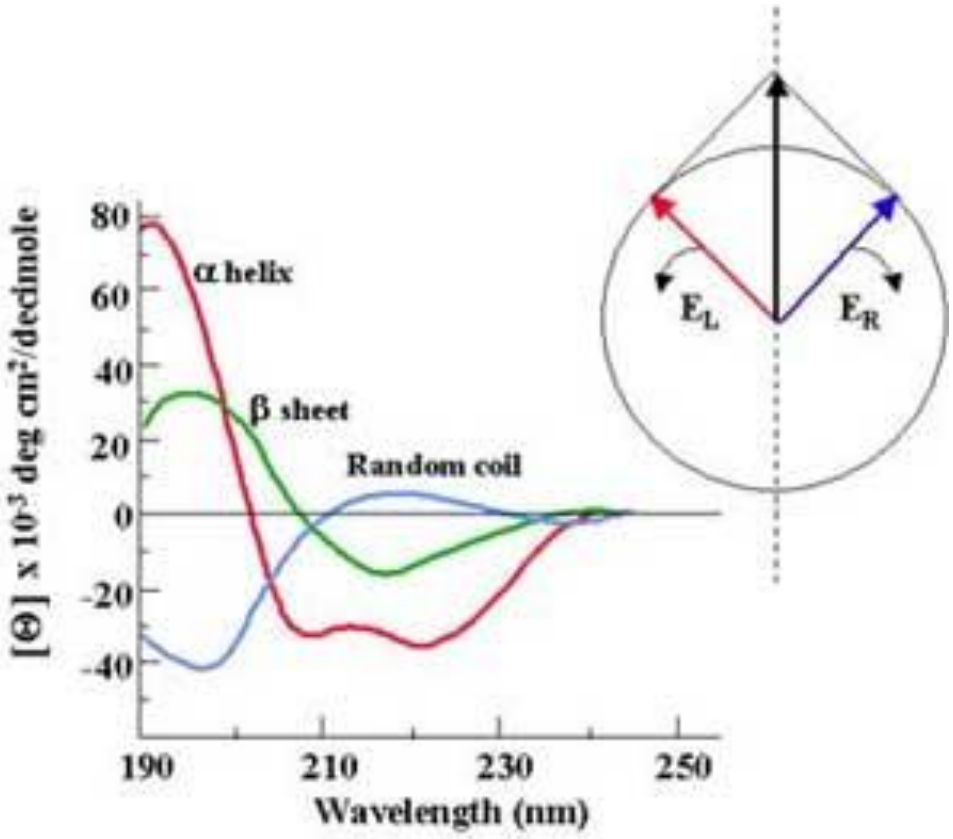

Figure 5: Typical CD spectra corresponding to different structures.

CHAPTER 3. MATERIALS AND METHODS

3.1 Materials

1-palmitoyl-2-oleoyl-phosphatidylcholine (POPC), dodecylphosphocholine (DPC), 1-palmitoyl-2-oleoyl-phosphatidylglycerol (POPG) and brominated lipids were purchased from Avanti Polar Lipids, Inc. Alabaster, AL. Bax peptides (Ac-VTIFVAGVLTASLTIWKKMG-NH2) along with two other mutants were from Biopeptide San Diego, CA. *Sephadex*® G-50 medium was from Amersham Biosciences (Uppsala, Sweden) and SM-2 Biobeads from Bio-Rad Laboratories (Hercules, CA). Analytical and highest purity chemicals from Sigma Aldrich Co. (St. Louis, MO). Calcein disodium salt from Fluka Analytical, Sigma Aldrich (St. Louis, MO) while polycarbonate filters for LUV preparation were purchased from Avastin, Inc. (Ottawa, Ontario, Canada).

3.2 Calcein Release Assay

Large Unilamellar Vesicles (LUVs), a model membrane system, were generated from a 10 mM suspension of a lipid mixture as described above. Dried lipid film was suspended in 10 mM calcein disodium salt in buffer and the mixture was then extruded through a pair of 200 nm polycarbonate filters 15 times (Rabzelj et al., 2008). Free calcein was removed from the calcein entrapped vesicles using Sephadex™ G-50 column. The buffer flow rate was maintained at 3 mL/min using Econo Pump (BioRad, Hercules CA) and calcein-loaded

vesicle fraction was collected. 150 µM solutions of all three peptide samples (Bax-KK, Bax-LL and Bax-EE) are prepared (Kaushik, Krishnan, Prausnitz, & Ludovice, 2001) in 6 mM DPC using 20 mM phosphate buffer, pH 7.2, containing 0.8 mM EGTA and 150 mM NaCl. The peptide/DPC sample was then diluted 10 times by adding to the calcein loaded vesicles to make it below its CMC (Fu & Singh, 1999). The increase in fluorescence due to calcein release from LUVs was measured between 500-550 nm (λ_{max} =513 nm) with an excitation wavelength of 490 nm on Jasco 810 spectropolarimeter at 37^{o}C every 20 s for 30 min (Bensikaddour et al., 2008; Fu, Lomneth, Cai, & Singh, 1998). Only calcein that leaked from vesicles emitted measurable fluorescence because calcein at high concentration within vesicles (i.e., 10 mM) self quenches (Fu and Singh, 1999). The minimum and maximum (100% leakage) fluorescence intensity corresponding to addition of pure DPC (0.6 mM) and 0.05% Triton X-100 to the vesicle sample was determined respectively (Lovell et al., 2008; Martínez-Senac et al., 2002).

3.3 Circular Dichroism and Fluorescence measurements

CD and fluorescence spectra of membrane-reconstituted peptides were measured using a J-810 spectrofluoropolarimeter (Jasco Corp., Tokyo, Japan), as described (Qin et al., 2004; Pande et al. 2006). In both cases, a 0.4 cm path-length rectangular quartz cuvette containing a magnetic stir bar and mounted in the temperature-controlled sample holder was used. For CD measurements, LUVs were prepared using pure POPC or a 7:3 combination of POPC/POPG, without Br_2PC. Tryptophan fluorescence of the peptides was monitored using excitation at 290 nm. The

excitation and emission slits were 4 nm and 10 nm, respectively. For CD and fluorescence measurements, 10 and 5 scans were co-added to obtain the average spectra. Measurements were conducted either at 20^{o}C or 37^{o}C as indicated.

3.4 ATR-FTIR Spectroscopy

3.4.1 Sample Preparation

Lipid-peptide samples for ATR-FTIR experiments were prepared using previously described methods (Goormaghtigh, 1999; Vigano et al., 2003) with slight modifications. Two µL of the peptide dissolved in DMSO at 12.5 mM was dried with compressed nitrogen and by desiccation. The dry sample was dissolved in ~20 µL of hexafluropropanol, and 125 µL of 10 mM lipid dissolved in $CHCl_3$ was added. The peptide-lipid solution at lipid-to-peptide molar ratio of 50:1 was carefully spread onto one surface of a ~7 cm^2 clean germanium plate with 45^{o} aperture angles and dimensions of 5×2×0.1 cm^3 (Spectral Systems, Irvington, NY). The sample was dried in a desiccator; the germanium plate was assembled in a home-made ATR sample holder, which was mounted into the FTIR spectrometer at a position corresponding to a 45^{o} incidence angle. This setting corresponds to approximately 20 internal reflections at one side of the plate. The thickness of the sample was evaluated to be ~1.6 µm, which is significantly thicker compared than the decay length of the evanescent field (~0.3 µm). After measurements of the dry sample at two polarizations, the germanium plate with the sample was subjected to D_2O vapors for 1 hr in a confined volume, and the spectra of the D_2O-humidified sample were collected. This was

followed by injection of a D_2O-based buffer (150 mM NaCl, 10mM Hepes, pD 6.8) into the ATR cell and additional spectra collected.

3.4.2 IR Spectroscopy

The signal/noise ratio of FTIR spectra was improved with 200 scans on a Bruker Vector 22 Spectrophotometer, which was purged continuously with dried air (del Mar Martínez-Senac, Corbalán-García, & Gómez-Fernández, 2001). The reference spectra were measured using a bare germanium plate or a sample prepared using plane lipid without any peptide. Atmospheric water humidity spectra were measured at both polarizations by collecting spectra at various times, using the bare germanium plate, and were used for clearing the sample spectra from noise generated by residual humidity, when necessary.

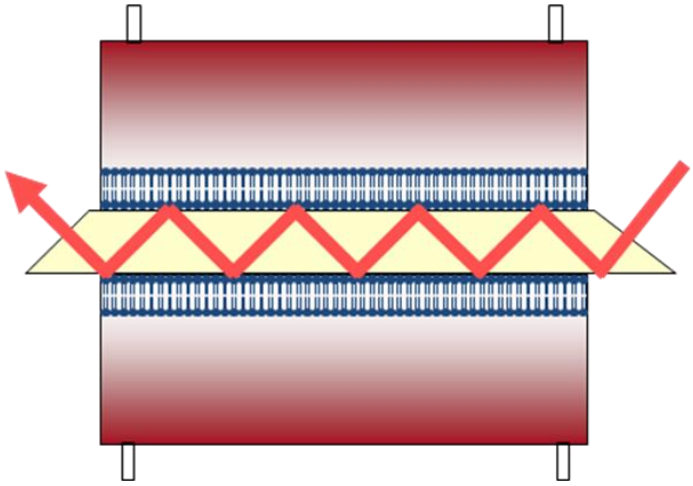

Figure 6: Internal Reflection of the infrared light within Ge plate creating an evanescent field at the surface where lipid-peptide are bound (Tatulian, 2003).

3.5 Membrane Insertion

LUV preparation: 100% POPC and 70% POPC and 30% POPG at 10 mM final concentration in chloroform. For each of the samples, 10 mol % of 6,7- 9,10- and 11,12- brominated lipids are also added to make the total lipid concentration of 1.2 mM (Bensikaddour et al., 2008). Chloroform was removed by evaporation with compressed nitrogen followed by vacuum desiccation for 1 hr. The lipid film was suspended in 0.5 mL of 20 mM phosphate buffer in H_2O, pH 7.2, containing 0.8 mM EGTA. LUVs are extruded by passing the lipid solution through the extruder with two 100 nm pore size filters and performing the extrusion 15 times to achieve the uniform vesicles (Ray, Scott, & Tatulian, 2007). 0.3 mM of peptide sample (Bax-KK, Bax-LL and Bax-EE) is taken from the stock in DMSO, solvent is removed under the stream of N_2 and vacuum desiccated again for 2 hrs. 9 mM DPC is added along with hexafluoroisopropanol (HFIP*)* to dissolve the peptides. The solvent again is removed by a stream of N_2 and suspended in 32 µL of 20 mM phosphate buffer (Rodionova et al., 1995). DPC is removed by vortexing the sample with SM-2 Biobeads (10% by weight) for 2 hrs.10 fold dilution of peptide/DPC sample is done in the vesicles so that it goes well below CMC (~1.5mM). Both CD and fluorescence with 290 nm excitation of Trp are measure at 20^oC and 37^oC.

CHAPTER 4. RESULTS

4.1 Calcein Release Assay

Studies on peptide-mediated calcein release from phospholipid vesicles are being conducted to see if the wild type and/or the mutant peptides are able to cause membrane destabilization and content release. Colum chromatography is performed using *Sephadex*® G-50 column, a constant flow rate of 3ml/min is maintained and 10 drops per tube are collected.

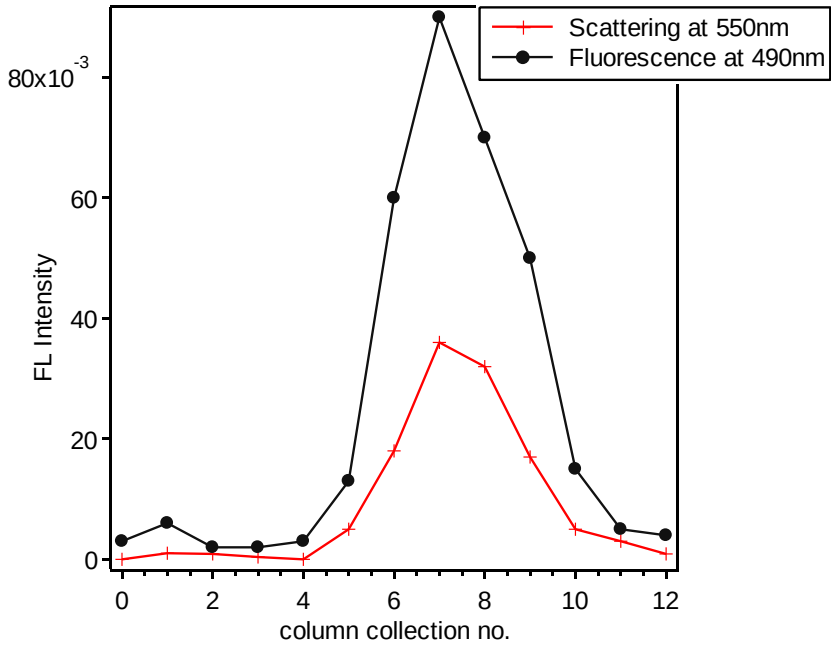

Figure 7: Fraction collection for 1 mM calcein-loaded-POPC vesicles using G-50 column at 25°C using 20 mM phosphate buffer containing 0.8 mM EGTA and 150 mM NaCl, pH 7.2

4.1.1 Calcein Release Assay with 100% POPC vesicles

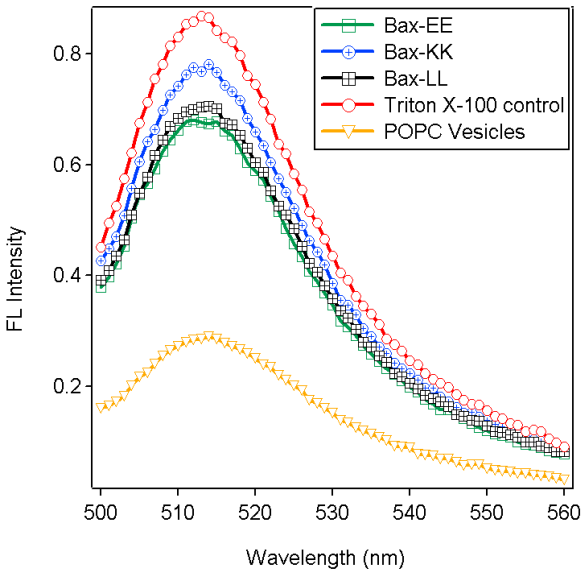

Figure 8: Bax mediated calcein release from POPC vesicles demonstrating differences in fluorescence intensity. Emission is measured between 500- 560 nm. Maximum intensity is seen at 513 nm. 0.05% Triton X-100 is used as positive control.

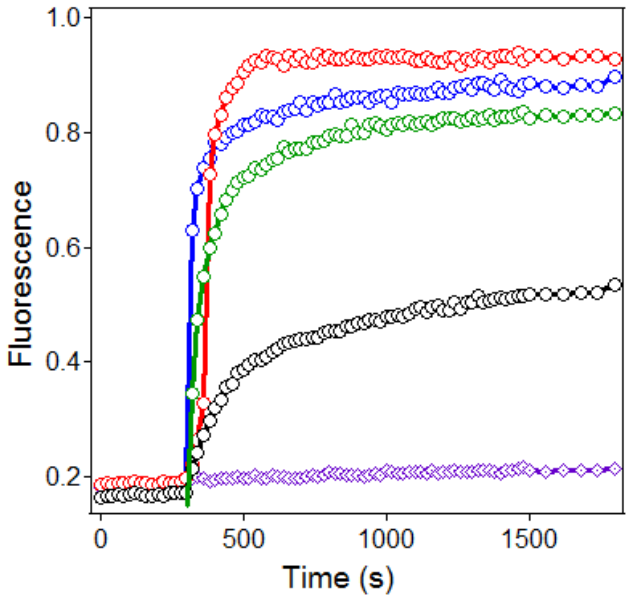

Figure 9: Fluorescence kinetics of entrapped 10 mM calcein release from vesicles prepared from 1 mM of POPC in 20 mM Phosphate buffer, pH 7.2. (Blue-Bax KK, Green: Bax-EE, Black: Bax LL, Red- Triton, Purple-DPC)

4.1.2 Calcein Release Assay with 70% POPC and 30% POPG

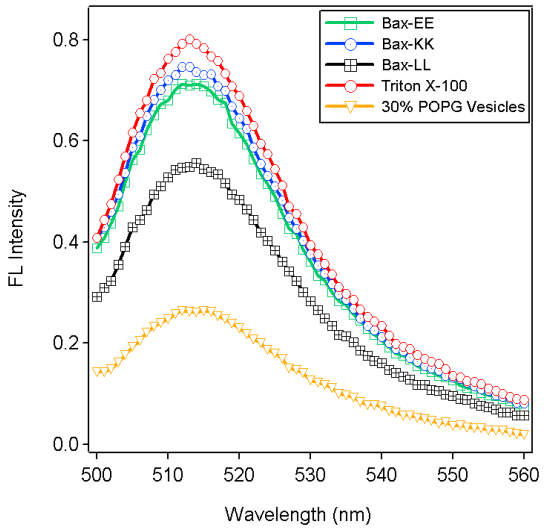

Figure 10: Bax mediated calcein release from 70% POPC + 30% POPG vesicles demonstrating differences in fluorescence intensity. Emission is measured between 500-560 nm. Maximum intensity is seen at 513 nm. 0.05% Triton X-100 is used as positive control.

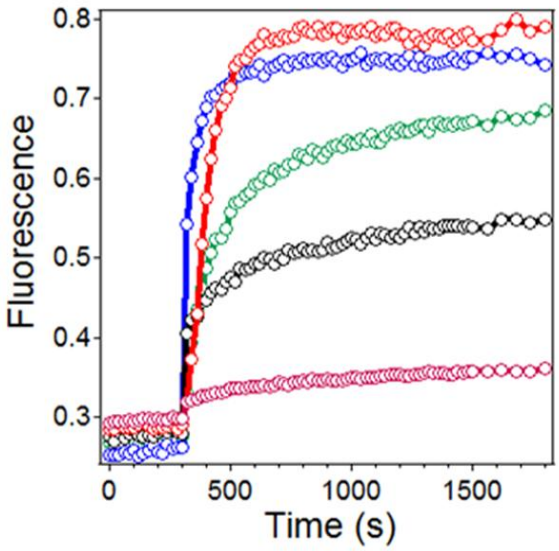

Figure 11: Fluorescence kinetics of entrapped 10 mM calcein release from vesicles prepared from 1 mM of POPC in 20 mM Phosphate buffer, pH 7.2. (Blue-Bax KK, Green: Bax-EE, Black: Bax LL, Red- Triton, Purple-DPC)

4.2 Membrane permeabilization by peptides

Calcein fluorescence is self-quenched at concentrations higher than ~1 mM (Rapaport et al., 1996; Park et al. 2006; Klocek et al. 2009). The concentration-dependence of calcein fluorescence is shown in Fig. 12A. If lipid vesicles are loaded with calcein at relatively high concentrations, then membrane permeabilization can be detected by calcein release into the large external compartment, resulting in calcein dilution, dequenching, and increase in fluorescence intensity. We used lipid vesicles 200 nm in diameter at 0.5 mM total lipid concentration loaded with 10 mM calcein. Using 4.0 nm for POPC or POPC/POPG membrane thickness (Vogel et al., 2000) and 0.68 nm^2 for cross-sectional area per lipid (Seelig et al., 1993), one can evaluate a 0.31 % fraction of vesicle-entrapped volume. Upon total disruption of the vesicles, calcein concentration in the external volume will increase from zero to ~0.03 mM, which corresponds to increase in fluorescence intensity to 1.0-1.1 relative units, as judged from data of Fig. 12A. Fig. 12B indicates a rapid increase in calcein fluorescence intensity upon addition of 1.667 μM of the wild-type peptide BaxC-KK. To ensure that calcein release from the vesicles was due to membrane pore formation rather than membrane disruption, vesicle integrity was estimated by right angle static light scattering on a J-810 spectrofluoropolarimeter. When incident light was used at 550 nm, slightly red-shifted light scattering from vesicles was detected (Fig. 12C). Addition of $1/10^{th}$ volume of buffer resulted in a ~10% decrease in intensity of scattered light due to dilution of the vesicle suspension. Addition of $1/10^{th}$ volume of plain DPC (at final DPC concentration of 0.6 mM) or any of the three peptides solubilized in DPC at final peptide concentration of 1.667 μM to15 μM did not result in any additional decrease in light scattering, indicating that neither the peptides nor DPC caused vesicle disruption. Triton X-100 caused

strong reduction of light scattering. The residual scattering was due to mixed Triton X-100-lipid micelles, indicating complete degradation of the vesicles by Triton X-100.

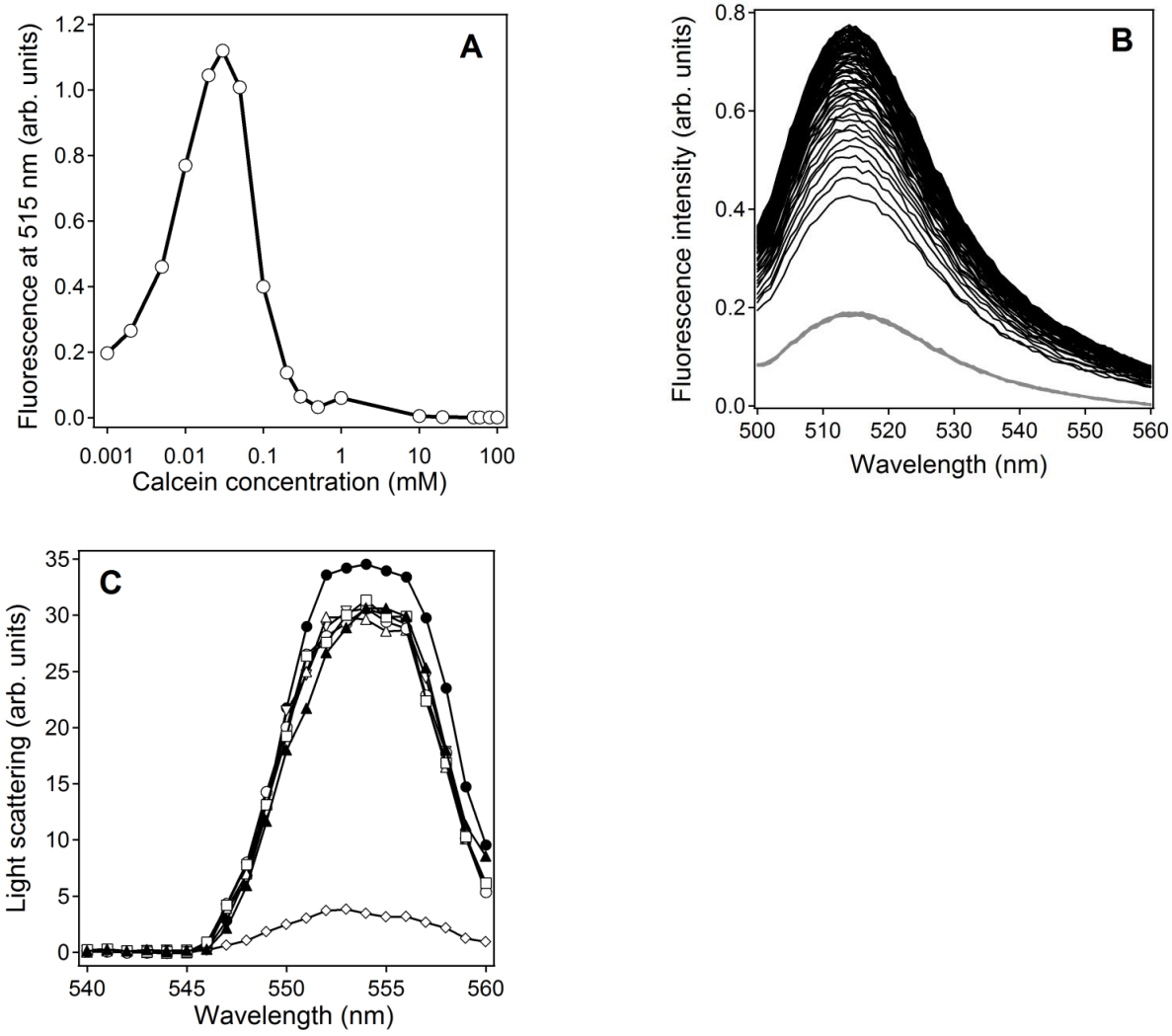

Figure 12: Calcein release experiments spectra showing (A) Calcein concentration curve, (B) increase in Fluorescence upon addition of Bax-KK and (C) Light scattering data pre (closed circles), post the addition of buffer (open triangles), the peptides, or Triton X-100 (rhombs).

4.3 Analysis of Pore formation kinetics

Following a previously described formalism for peptide-mediate membrane pore formation, we propose that introduction of peptide into LUVs results in rapid insertion of the peptide followed by membrane destabilization and a slower process of formation of the final structure of the pore. In case of the wild type peptide, the fast and slow components are characterized with time constants of 10-30 s and 20-10 min, respectively, which are likely related to these processes. Upon membrane binding of the peptides and pore formation, the observed calcein fluorescence increases from zero to equilibrium value F_{eq}. If eventually every peptide contributes to pore formation, then the concentration of free peptide at time t, $[P]_t$, can be expressed through the total peptide concentration, $[P]_0$, and fluorescence intensity at time t, F_t, as follows:

$$[P]_t = [P]_0 \left(1 - \frac{F_t}{F_{eq}} \right) \quad (1)$$

Given the hydrophobic nature of the peptides and their poor water solubility, it is reasonable to assume that nearly all of the peptide is membrane bound. We use a model of pore formation where peptide molecules associate with each other in a stepwise fashion to form an oligomeric assembly. If the pore is composed of $n \geq 2$ peptide molecules, then addition of each molecule can be considered a second-order process that is described as follows:

$$\frac{1}{[P]_t} - \frac{1}{[P]_0} = k_a t \quad (2)$$

where k_a is the second-order association rate constant in units $M^{-1}s^{-1}$. Combination of Eqs. (1) and (2) yields:

$$\frac{F_{eq}}{[P]_0\left(F_{eq}-F_t\right)}=\frac{1}{[P]_0}+k_a t \tag{3}$$

Equation (3) indicates that the second-order rate constant of pore formation, k_a, can be determined as the slope of the time dependence of the term at left-hand side of Eq. (3). Values of F_{eq} are tabulated in Table 2.

Generally, a bimolecular process where reactants *A* and *B* combine in a complex *AB*, which then either dissociates to *A* and *B* or leads to the formation of the final product *P*, can be describe as shown in Scheme 1:

$$A+B \underset{kd}{\overset{ka}{\Leftrightarrow}} AB \overset{kp}{\rightarrow} P$$

Scheme 1

Here, k_a and k_d are the forward and reverse rate constants of complex formation, and k_p is the rate constant of product formation. The effective (observed) rate constant of product formation is

$$k_{eff}=\frac{k_a k_p}{k_p+k_d} \tag{4}$$

Two cases can be considered. First, product formation is much faster than complex dissociation ($k_p >> k_d$). This leads to:

$$k_{eff} \approx k_a \tag{5}$$

Second, complex dissociation is much faster than product formation ($k_p << k_d$). This leads to:

$$k_{eff} \approx \frac{k_a k_p}{k_d} = K k_p \tag{6}$$

Here, K is the peptide-peptide association constant in units M^{-1}.

The oligomeric state of the pore, i.e. the number of peptide monomers per pore, can be estimated using a formalism of reversible aggregation (Nir, Nieva. 2000, Nieva, 2003). This model is applicable to general cases when the sample contains j = 1 to S different types of vesicles, such as vesicles of different size categories, and each vesicle of type j contains up to N_j peptide molecules. If the number of peptides per pore is n, then only vesicles containing peptides $i = n$ to N_j ($n \le i \le$ Nj) will leak. The fraction of leakage reached at $t \to \infty$ (F_{eq}, see above) relative to the maximum possible leakage (F_{max}, caused by vesicle disruption by Triton X-100), is given as:

$$F_{rel} = \frac{F_{eq}}{F_{max}} = \left[q^{n-1} \left(n - nq + q \right) \right] \sum_{i=n}^{N_j} \sum_{j=1}^{S} A_{i,j} f_j \tag{7}$$

where

$$q = \frac{1}{\alpha + \sqrt{\alpha^2 - 1}} \tag{7a}$$

$$\alpha = 1 + \frac{1}{4K[P]_0} \tag{7b}$$

In Eq. (7), $A_{i,j}$ is the normalized fraction of vesicles of size j that contain i bound peptides, and f_j is the fraction of encapsulated volume of vesicles of type j normalized relative to the total encapsulated volume. Considering that the vesicles used in this work have been extruded through membranes of defined pore size (200 nm), only one type of vesicles can be considered, i.e., S = 1. Furthermore, it is reasonable to assume that all vesicles contain similar numbers of peptides, i.e. the average number of peptide molecules per vesicle. Under our experimental conditions (total lipid concentration of 0.5 mM and peptide concentrations of 1.667 μM, 5.0 μM, and 15.0 μM), this number varied between 1180 and 10650, which is much larger than any conceivable number of peptide molecules per pore. With these considerations, we arrive at

$$\sum_{j=1}^{S} f_j = 1 \quad \text{and} \quad \sum_{i=n}^{N_j} A_{i,j} = 1 \tag{8}$$

Combination of Eqs. (7) and (8) yields:

$$F_{rel} = q^{n-1}(n - nq + q) \tag{9}$$

If experiments of vesicle content release are performed at various peptide concentrations, then the experimental values of F_{rel} can be determined at each concentration and compared with those calculated through Eq. (9) using different values for n. Values of n at which the calculated and

measured values of F_{rel} merge can be used as the number of peptide molecules per pore. It should be noted that this procedure of determination of n is more accurate than the model considering an irreversible aggregation, in which overestimated values of n are obtained (Parente et al, 1990). Furthermore, the calculated value of F_{rel} does not depend on the fraction of membrane-bound peptide. If the fraction of membrane-bound peptide decreases x times, the slope of the linear relationship given by Eq. (3), and hence k_a, and consequently K (Eq. 6) increase x times. Thus, in Eq. (7b) a certain change in membrane-bound peptide concentration $[P]_0$ is compensated by an opposite change in K, resulting in no change in values of q (Eq. 7a) and F_{rel} at a given n. This indicates that using the experimental values of the total peptide concentration for $[P]_0$ does not introduce error in evaluated parameters of pore formation.

Table 2: Kinetic parameters of calcein release from vesicles composed of 100% POPC (PC) or 70% POPC + 30% POPG (PC/PG) derived from fitting the data with a double-exponential equation: $F_t = F_{eq} – a_1\exp(-k_1t) – a_2\exp(-k_2t)$, where F_t is calcein fluorescence intensity at time *t*, F_{eq} is the fluroscence at $t\rightarrow\infty$, k_1 and k_2 are the rate constants. C_p is the total peptide concentration in μM.

C_p	F_{eq}		a_1		a_2		k_1 (s^{-1})		k_2 (s^{-1})	
	PC	PC/PG	PC	PC/PG	PC	PC/PG	PC	PC/PG	PC	PC/PG
	BaxC-KK									
1.667	0.5622	0.5969	0.2974	0.1917	0.2633	0.3724	0.002939	0.001936	0.086286	0.038464
5.0	0.6224	0.6312	0.1722	0.2236	0.4508	0.3949	0.002589	0.002632	0.105304	0.050731
15.0	0.6920	0.6726	0.1555	0.1618	0.5283	0.5078	0.0035407	0.005551	0.074997	0.115064
	BaxC-EE									
1.667	0.3811	0.2555	0.1652	0.1175	0.2008	0.1387	0.001164	0.000817	0.000401	0.002029
5.0	0.5912	0.6078	0.4165	0.4592	0.1784	0.1529	0.001362	0.001256	0.015592	0.008628
15.0	0.7075	0.7020	0.2238	0.2382	0.4733	0.4596	0.003443	0.003539	0.025874	0.015385
	BaxC-LL									
1.667	0.2076	0.3264	0.1244	0.2412	0.07143	0.0784	0.000629	0.001130	0.004593	0.007391
5.0	0.2781	0.5085	0.2002	0.3918	0.07003	0.1085	0.001035	0.000573	0.017925	0.011937
15.0	0.3969	0.6134	0.1933	0.2302	0.2013	0.3390	0.001136	0.001239	0.010174	0.000376

Now once the double exponential constants are calculated, there is need to evaluate the degree of affinity between those peptide molecules. For this purpose the affinity constants are calculate. The rate constants k_{a1} and k_{a2} shown in Table 3 are 10^3-10^4-fold smaller than the estimated value of k_{diff}, indicating that the pore formation is much slower than a simple diffusion-controlled process. This in turn implies that in most cases peptides can diffuse away from each other before the complex is formed. Thus, the rate constant of peptide complex formation, k_p, is the rate-determining step, and therefore, according to Eq. 6, $k_{eff} = Kk_p$. Here, k_{eff} is the observed second-order rate constant, i.e. those summarized in Table 3 as k_{a1} and k_{a2}, K is the peptide-peptide binding constant, and k_p is the rate constant of peptide complex formation. Analysis of the kinetic data on peptide-induced vesicle content leakage indicates rapid membrane binding of the peptide, with time constants in the range of seconds, followed by two distinct processes that can be described using bimolecular rate constants of 5000-9000 $M^{-1}s^{-1}$ at 5-10 min following peptide addition and 20000-40000 $M^{-1}s^{-1}$ at later times (Table 3). The process taking place at earlier times likely reflects the nucleation of the pore complex, which is the rate-limiting step of pore formation, and is characterized with peptide-peptide affinity constants of $K_1 = (1.3\text{-}3.7)\times10^6$ M^{-1}. The second process is interpreted in terms of formation of the final pore structure, which proceeds at a 4-fold higher speed and results in peptide-peptide association with affinity constants of $K_2 = (0.5\text{-}1.4)\times10^7$ M^{-1} (Table 3). These results for the mutant peptides fit well with the model for initial nucleation of the pore structure, including 2-3 peptide molecules, and further progression of the process to the final pore structure that can probably contain a varying number of peptide molecules which appears to be limited by of $n = 8$ molecules per pore (see below for more detail on the mechanism of pore formation).

Table 3: The fraction of maximum possible vesicle content leakage (F_{rel}), second-order rate constants (ka_1 and ka_2), and peptide-peptide affinity constants (K_1 and K_2) characterizing membrane pore formation by the peptides. Parameters k_{a1} and K_1 were derived from the data for initial time period (5-10 min) following addition of peptides to the vesicles, while k_{a2} and K_2 were derived from data corresponding to later times (~ between 10-20 min). C_p is the total peptide concentration in μM.

C_p	F_{rel}		k_{a1} ($M^{-1}s^{-1}$)		k_{a2} ($M^{-1}s^{-1}$)		K_1 (M^{-1})		K_2 (M^{-1})	
	PC	PC/PG	PC	PC/PG	PC	PC/PG	PC	PC/PG	PC	PC/PG
						BaxC-KK				
1.667	0.755	0.843	8966	7190	41800	21407	3.05×10^6	3.71×10^6	1.42×10^7	1.11×10^7
5.0	0.836	0.892	4459	4608	34090	19538	1.72×10^6	1.75×10^6	1.31×10^7	7.42×10^6
15.0	0.929	0.950	4871	7318	21973	26868	1.37×10^6	7.71×10^5	6.21×10^6	4.84×10^6
						BaxC-EE				
1.667	0.513	0.332	552	1276	1092	2267	4.74×10^5	1.56×10^6	9.38×10^5	2.77×10^6
5.0	0.796	0.789	710	594	1672	1010	5.21×10^5	4.73×10^5	1.23×10^6	8.04×10^5
15.0	0.952	0.912	1852	2389	6892	8156	5.38×10^5	6.75×10^5	2.00×10^6	2.30×10^6
						BaxC-LL				
1.667	0.317	0.407	1208	1526	---	2748	1.92×10^6	1.35×10^6	---	2.43×10^6
5.0	0.425	0.634	598	243	---	---	5.77×10^5	4.24×10^5	---	---
15.0	0.606	0.765	373	70	---	---	3.28×10^5	1.87×10^5	---	---

4.4 The Structure of Membrane-Bound Peptides by ATR-FTIR

The peptide sample was mixed with two different lipids and deposited on the Germanium plate. The lipid-peptide sample was subjected to three different environmental conditions. Every measurement is done at two polarizations of the infrared light with respect to the plate, which are used to obtain a polarization independent spectrum as $A=A_{\parallel} + 1.44A_{\perp}$. This spectrum is then processed for second derivative determination and finally curve fitted to evaluate the secondary structure determination. All the electric field components of the evanescent field need to be taken into consideration (Marsh et al, 1999). The polarized spectra were used to calculate the dichroic ratios and then the orientations of membrane-bound peptides.

Curve fitting is performed for the polarization independent spectra for each of the three cases of dry, vaporized and buffer peptide sample. The curve fitting results for ATR-FTIR indicate that the minimally hydrated samples of peptides in stacked lipid bilayers (absence of bulk water) were mostly α-helical but adopted mostly β-sheet conformation in the presence of excess water. Hence a larger peak around ~1627 cm^{-1} is seen in hydrated samples indicating the transformation into more β-sheets.

4.4.1 Bax KK

The wild type Bax peptide is first measured using dry lipid film on the Ge plate. Then the sample hydrated with D_2O vapors and finally flushed with D_2O buffer to determine the change in the secondary structure upon various environments. Increase in β-sheet structure was identified upon exposure of the sample to bulk aqueous phase.

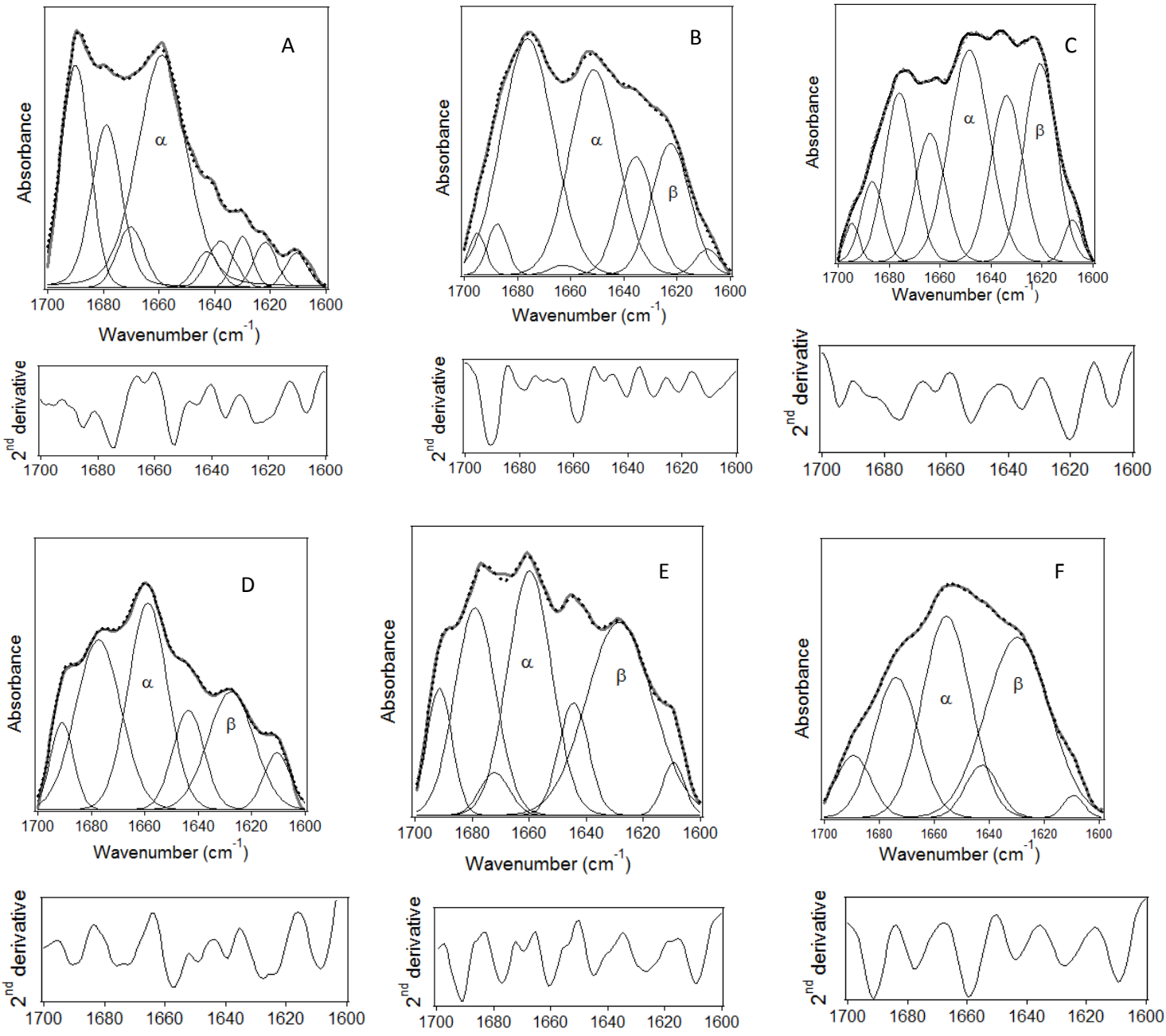

Figure 13: ATR-FTIR spectra for Bax KK in 100% POPC (A-C) and 70% POPC and 30% POPG (D-F) films deposited on the Ge plate in the absence hydration (A, D), exposed to D_2O vapor for 1 hr (B, E), and in the presence of bulk D_2O-based buffer (C, F).

The dry sample has a greater percentage of α helix in its secondary structure (A, D) compared to when the sample is hydarated with D_2O vapors for an hour (B, E). A greater peak is seen around 1624 implying an increase in the percentage of β sheets after vaporization. Finally the hydrated sample (C, F) have very large β sheets implying more β sheet formation after D_2O buffer hydration.

As we can see that an iterative curve fitting between 1700 and 1600 cm^{-1} is a very important tool in order to determine the area of amide I components. All the peaks generated during curve fitting are based on secondary derivatives and hence closely correspond to various secondary structures present in the peptide at that given environmental condition. Three different conditions would yield three different ATR-FTIR spectra which were individually curve fitted. Sum of all the peaks would give the entire amide I region and is called a ‘fitted peak’. Finally the percentage of one particular secondary structure present in the peptide can be calculated by dividing its peak area by the total area of amide I region.

4.4.2 Bax EE

The mutant Bax EE is also measured using dry lipid film on the Ge plate. Then the sample was hydrated with D_2O vapor and finally flushed with D_2O buffer to determine the change in the secondary structure upon various environmental changes. Again, excess water caused the peptide to adopt a mostly β-sheet conformation.

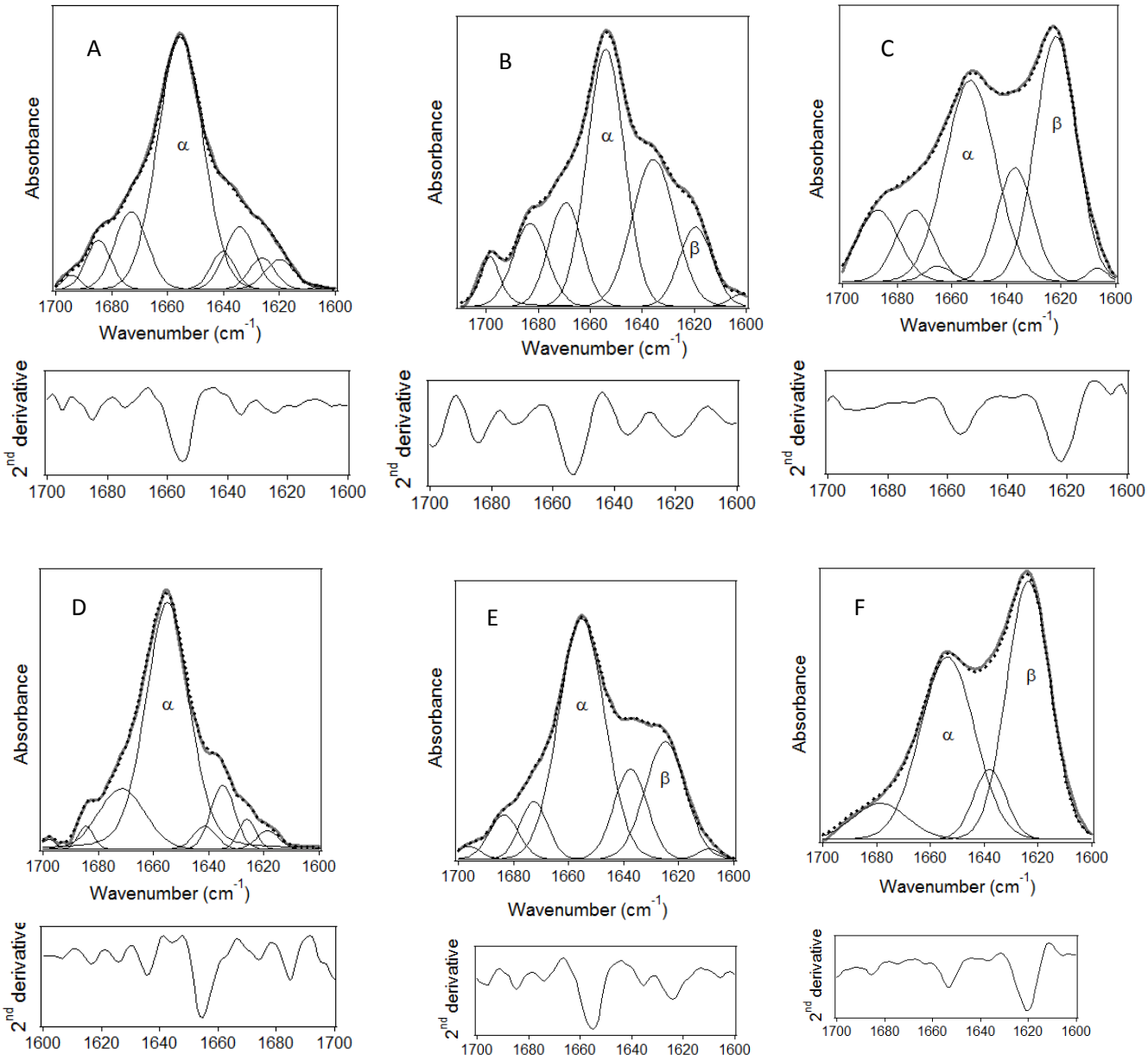

Figure 14: ATR-FTIR spectra for Bax EE in 100% POPC (A-C) and 70% POPC and 30% POPG (D-F) films deposited on the Ge plate in the absence hydration (A, D), exposed to D_2O vapor for 1 hr (B, E), and in the presence of bulk D_2O-based buffer (C, F).

4.4.3 Bax LL

The mutant Bax LL is also measured using dry lipid film on the Ge plate. Then the sample was hydrated with D_2O and finally flushed with D_2O buffer to determine the change in the secondary structure upon various environmental changes.

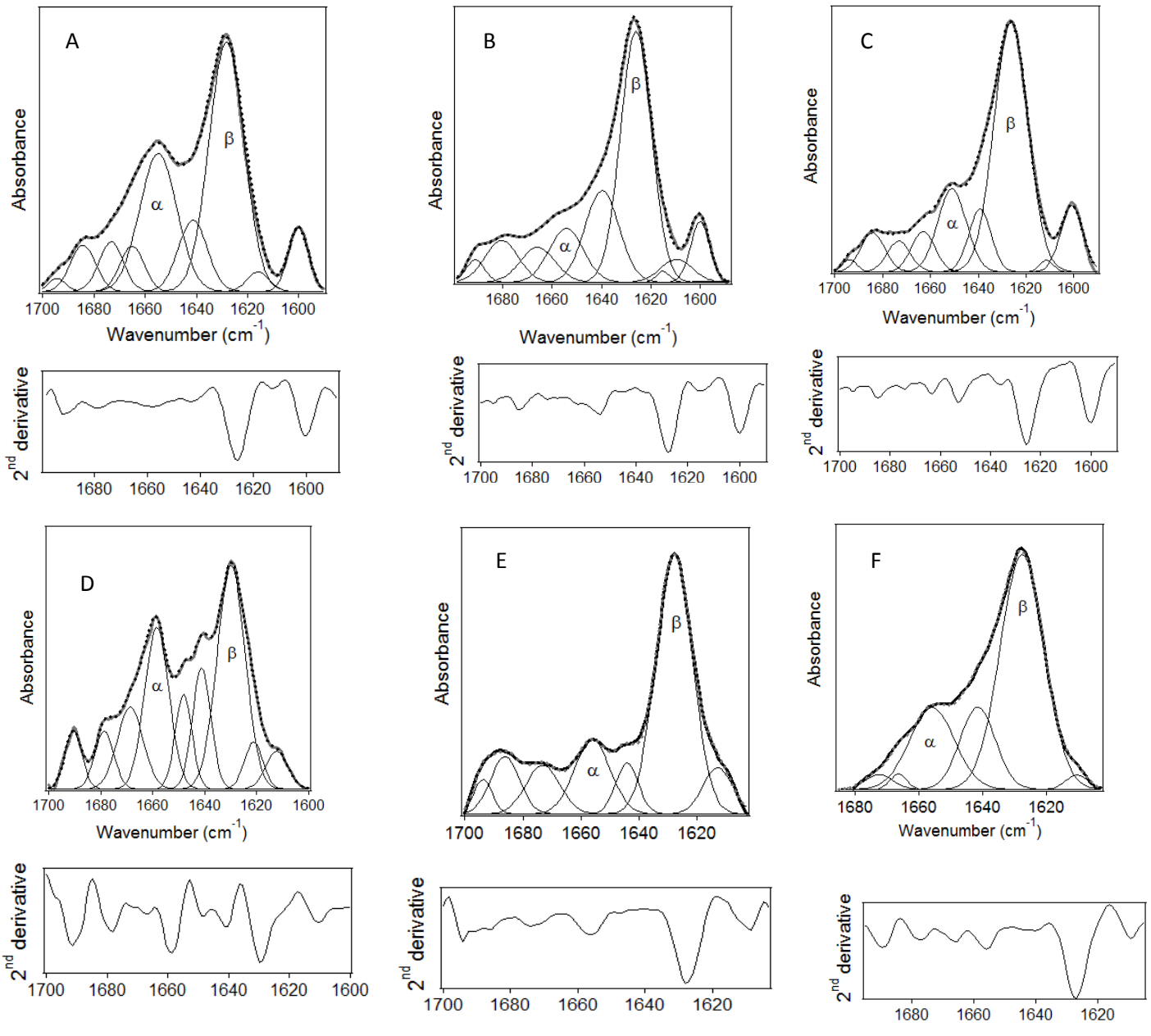

Figure 15: ATR-FTIR spectra for Bax LL in 100% POPC (A-C) and 70% POPC and 30% POPG (D-F) films deposited on the Ge plate in the absence hydration (A, D), exposed to D_2O vapor for 1 hr (B, E), and in the presence of bulk D_2O-based buffer (C, F).

Note: Bax LL peptide was rich in β-sheet structure under all conditions.

Table 4: Fractions of alpha helix and beta sheet structures in peptides from ATR-FTIR data along with the standard deviations.

	Bax-KK		**Bax-EE**		**Bax-LL**	
	α	β	α	β	α	β
POPC	0.264+/-0.001	0.198+/-0.003	0.334+/-0.067	0.325+/-0.013	0.142 +/-0.045	0.508+/-0.271
POPC/POPG	0.306+/-0.0217	0.361+/-0.023	0.356+/-0.002	0.454+/-0.001	0.203+/-0.001	0.571+/-0.001

4.5 Confirmation by Circular Dichroism

It has now been shown by the ATR-FTIR experiments that Bax peptides assume more β-sheet confirmation in the presence of bulk water. This idea was confirmed by CD experiments where peptides were dissolved in aqueous buffer and readings were taken to study their secondary structure. The β-sheets always give a minimum around 215 nm which was a characterizing feature in all these spectra.

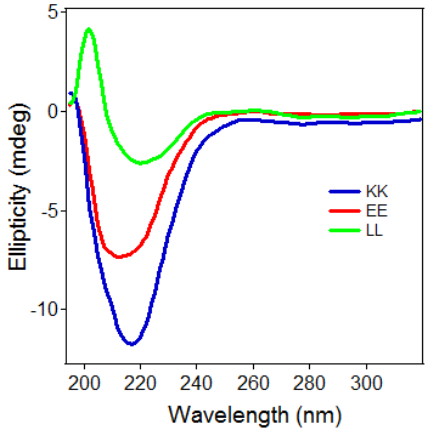

Figure 16: Structural analysis by CD confirming the mostly β-sheet secondary structure of Bax Peptides.

4.6 Depth of Membrane Insertion

Depth of membrane insertion was determined at both 20°C and 37°C by fluroscence quenching of *Trp* by dibromo-phosphatidylcholines (Br_2PCs). The effect of membrane charge was studied by using pure 1-palmitoyl-2-oleoyl-phosphatidylcholine (POPC) and 70% POPC + 30% 1-palmitoyl-2-oleoyl-phosphatidylglycerol (POPG) in membrane preparations with and without Br_2PCs brominated at 6,7-, or 9,10-, or 11,12 positions of the acyl chains.

4.6.1. Fluorescence Spectra

The depth of membrane insertion was determined as described previously (Ray et al, 2007).

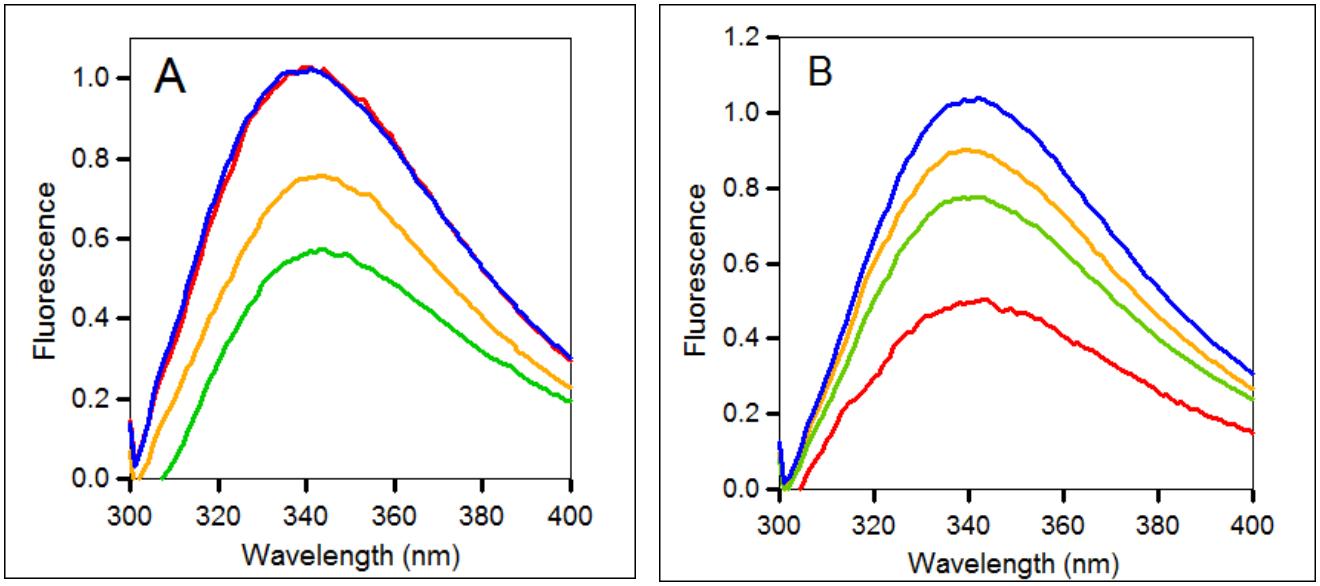

Figure 17: Fluorescence of Bax-KK measured using excitation at 290 nm, at 37^{o}C. Pure POPC (left) and 70% POPG + 30% POPG (right) are compared using same concentrations of brominated lipids. (Blue- Pure Lipid, Orange- 6,7 Br_2PC, Green- 9,10 Br_2PC, Red- 11,12 Br_2PC)

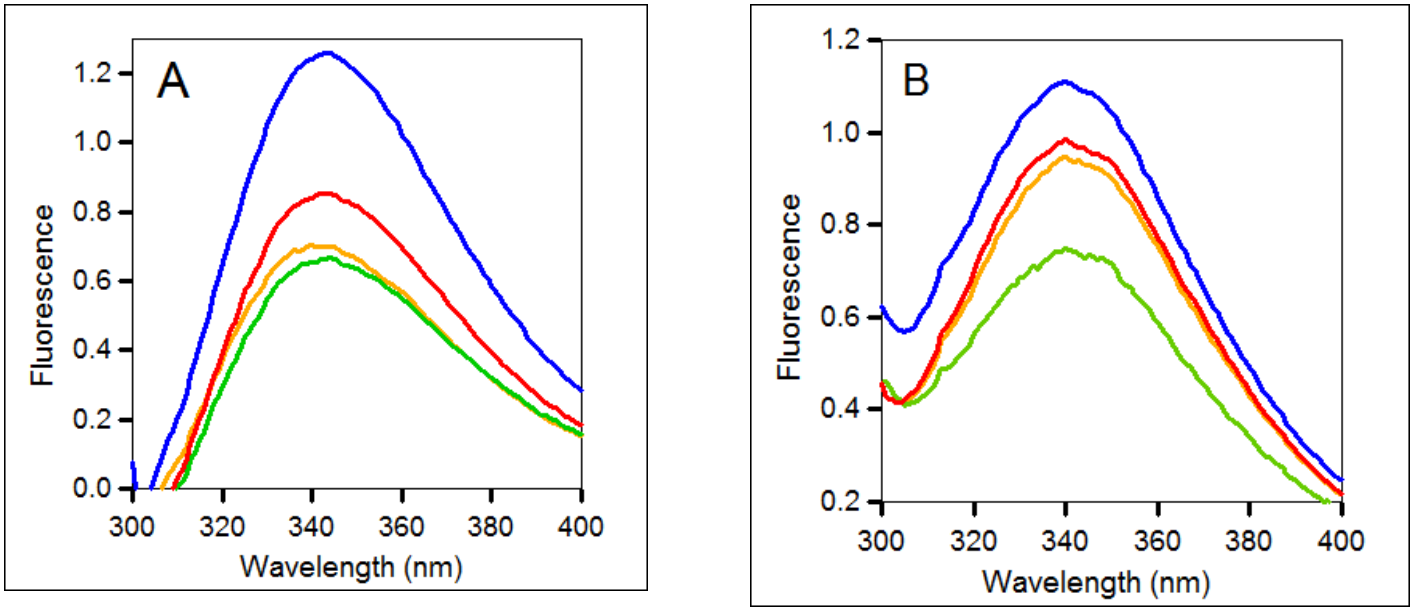

Figure 18: Fluorescence of Bax-EE measured using excitation at 290 nm, at 37°C. Pure POPC (left) and 70% POPG + 30% POPG (right) are compared using same concentrations of brominated lipids. (Blue- Pure Lipid, Orange- 6,7 Br_2PC, Green- 9,10 Br_2PC, Red- 11,12 Br_2PC)

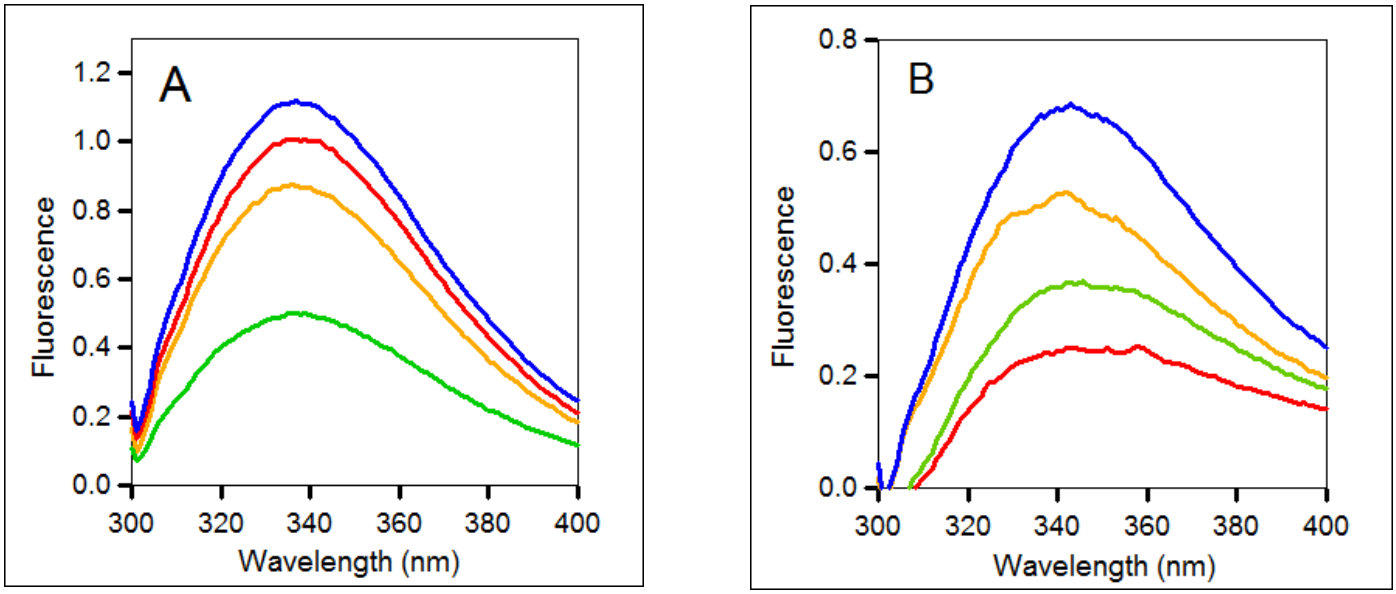

Figure 19: Fluorescence of Bax-LL measured using excitation at 290 nm, at 37°C. Pure POPC (left) and 70% POPG + 30% POPG (right) are compared using same concentrations of brominated lipids. (Blue- Pure Lipid, Orange- 6,7 Br_2PC, Green- 9,10 Br_2PC, Red- 11,12 Br_2PC)

4.6.2. Distribution Analysis

"Distribution analysis" of the experimental data was determined by the formulation as shown in equation (10):

$$\ln \frac{F_0}{F} = \frac{S}{\sigma(2\pi)^{1/2}} \exp\left[-\frac{(h-h_m)^2}{2\sigma^2}\right] \quad (10)$$

Where F_0 is the fluorescence intensity without and F the intensity with quencher; S is the area and σ the dispersion of the distribution curve; and h is the distance and h_m is the most probable distance from the membrane center (Ray et al, 2007).

The final concentration of Bax that was added to the suspension after preparation of the vesicles was 30 μM. Lipid and protein concentrations ensured that most of the protein was bound to the membranes. Spectra of blank buffer were measured as references and used for correction by subtracting from the sample spectra. Samples were thermostated at each temperature for 5 min before the spectra were recorded, with constant stirring by a magnetic stir bar in a 0.4 cm path length quartz cuvette. The three values of ln (F_0/F), which were obtained with three different Br_2PCs, were plotted as a function of the distance of bromines in Br_2PCs from the membrane center, i.e., 11.0, 8.3, and 6.5 Å for 6,7-, 9,10-, and 11,12-Br_2PC respectively as shown in Fig 20. Fitting of these data by Eq. (10) allowed determination of parameters S, σ, and h_m.

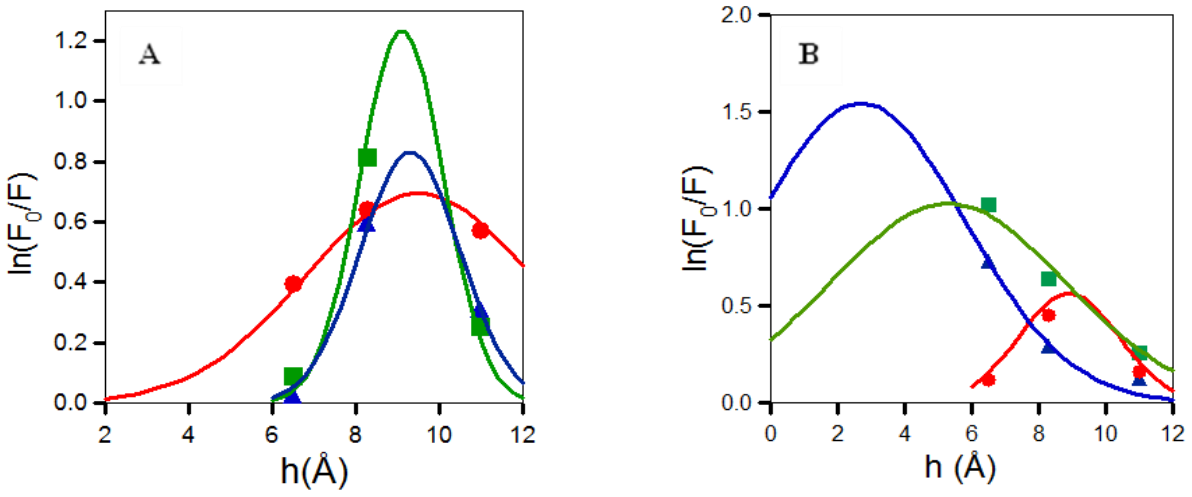

Figure 20: "Distribution analysis" of all three peptides was performed using the equation which results in individual fitted curves for pure POPC (A) and with 70% POPG + 30% POPG (B) lipid compositions (Blue: Bax-KK, Green: Bax-LL, Red: Bax-EE).

Table 5: The "distribution analysis" parameters of various Bax mutants in two different lipid compositions.

	Bax-LL			**Bax-KK**			**Bax-EE**		
	S	**σ**	**h_m**	**S**	**σ**	**h_m**	**S**	**σ**	**h_m**
POPC (no POPG)	3.1	1.0	9.1	2.5	1.2	9.3	4.7	2.7	9.5
POPC+ 30% POPG	9.0	3.5	5.3	12.0	3.1	2.7	2.1	1.49	8.9

CHAPTER 5. DISCUSSION

Insertion of Bax into mitochindrial membrane is the hallmark of Apoptosis. The solution structure of Bax has been solved (Torrecillas et al, 2008). However the exact mechanism of its function is still unknown. For this reason elucidation of secondary structure and mode of insertion becomes most important. With the calcein release experiments, it is established that Bax C-terminal peptide is able to form pores in lipid membranes and cause vesicle content release. Given the hydrodynamic radius of calcein of 0.64 nm, the pore has a diameter of at least 1.3 nm or larger. Wild type Bax KK has the highest penetration in the lipid vesicles. However for pure POPC membranes, Bax LL releases more calcein than vesicles made with 30% anionic lipids. Once we have established that different peptides have different rupture powers for the lipid vesicles, we conducted structural studies to elucidate the molecular basis for membrane pore formation by the peptides. Using brominated lipids the position of tryptophan is determined and it is seen that for pure POPC membranes, Trp16 is around 9.3 Å from the membrane center and our results are consistent for all three peptides. However for 30% POPG, Trp16 was inserted much deeper; h_m was seen to be around 2.7 and 5.3 Å for wild type and Bax-LL peptides respectively but was at $h_m \approx 9$ Å for the Bax-EE peptide. Thus, the wild type Bax peptide has the highest membrane insertion and the strongest membrane perforation potency, which may play a role in pore formation in mitochondrial membranes by Bax and cytochrome c release.

Peptides applied to calcein-loaded vesicles resulted in gradual increase in calcein fluorescence, apparently induced by membrane permeabilization by the peptides and calcein release (Fig. 21). While the kinetics and the level of calcein release were dependant on specific peptide, and its molar concentration as well as the lipid composition of vesicle membranes. All traces of time-dependence of calcein fluorescence could be fitted with $F_t = F_{eq} - a_1\exp(-k_1t) - a_2\exp(-k_2t)$, where F_t is calcein fluorescence intensity at time t, offset by subtraction of the fluorescence before peptide addition, F_{eq} is the extrapolated level of fluorescence at $t \rightarrow \infty$, a_1 and a_2 are the fractions of the two kinetic components, and k_1 and k_2 are the respective rate constants.

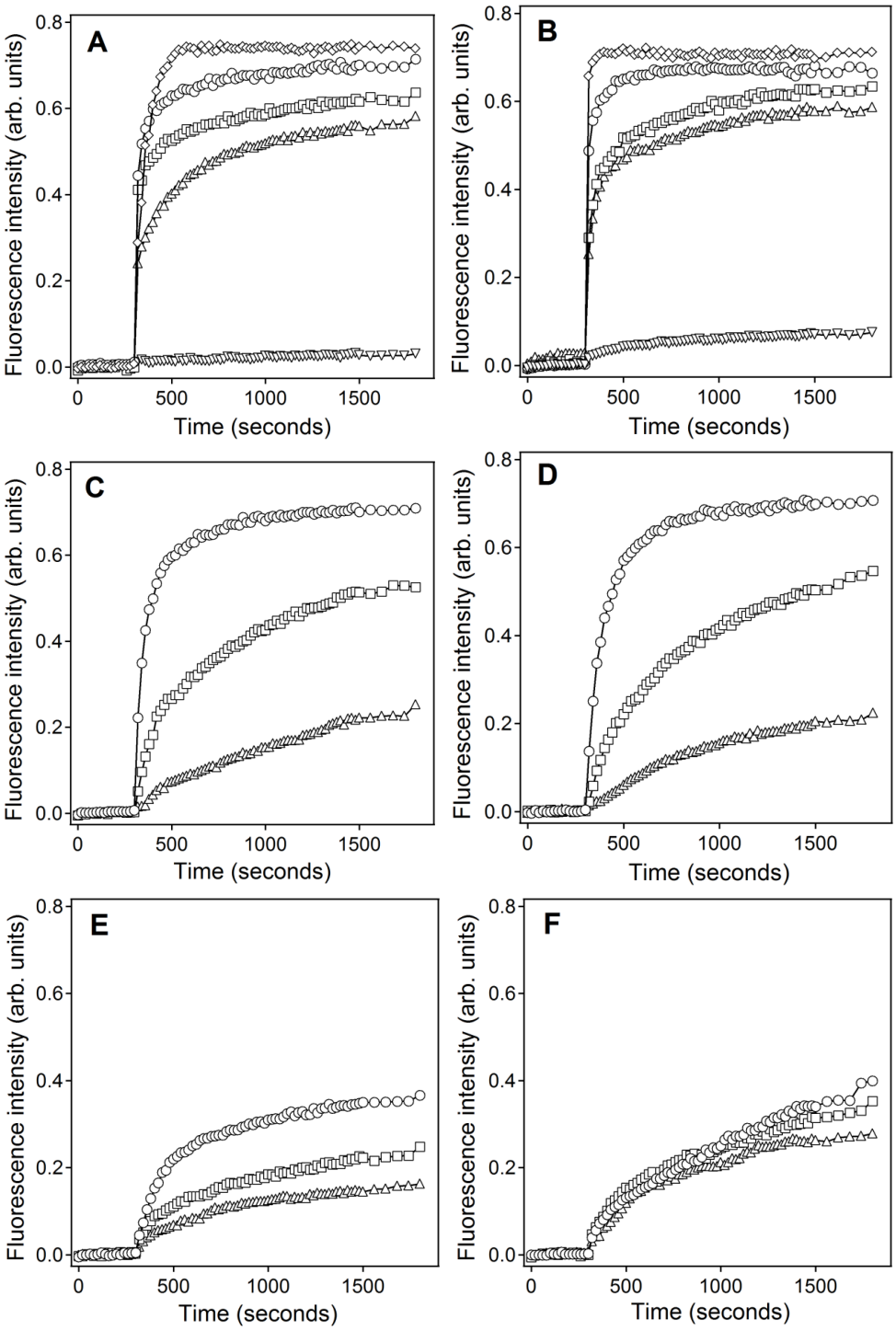

Figure 21: Addition of the peptides to calcein-loaded vesicles resulted in gradual increase in calcein fluorescence, apparently induced by membrane permeabilization by the peptides and calcein release.

Data of Fig. 22 indicate an initial linear time dependence of $F_{eq}/\{[P]_0(F_{eq} - F_t)\}$,characteristic of a bimolecular reaction, followed by a second segment of linear dependence with a higher slope at $t \geq 10$ min (for POPC/POPG vesicles and 15 μM peptide the second segments starts earlier). The data points corresponding to the second linear segment involve considerable noise because with increasing time F_t approaches F_{eq} and the values of $F_{eq}/\{[P]_0(F_{eq} - F_t)\}$become progressively unstable as the denominator decreases. Two linear segments of the graphs indicate that at least two processes are involved in membrane pore formation. If membrane binding of the peptide is relatively fast, as suggested by the 10-30 s time constant of the fast component of the double-exponential curves for BaxC-KK, then both linear segments of the graphs of Fig. 22 should be interpreted in terms of interactions between the peptide molecules within the membrane.

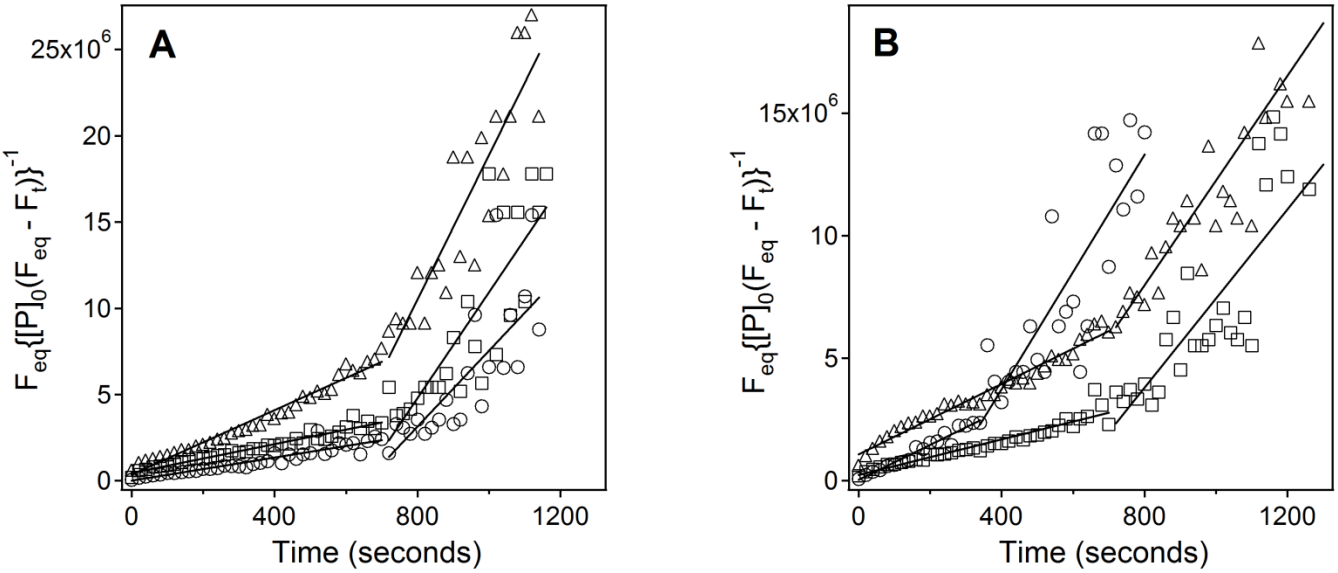

Figure 22: Spectra indicate an initial linear time dependence characteristic of a bimolecular reaction, followed by a second segment of linear dependence after addition of BaxC-KK peptide to the calcein-loaded vesicles.

The final step in characterization of pore formation is evaluation of the oligomeric state of the pore. This was achieved using a model of reversible aggregation that has been applied previously to describe membrane pores formed by other peptides (Nir, Nieva. 2000, Nieva, 2003). The mechanism of pore formation was analyzed using the slower double-exponential rate constants, which are believed to reflect the kinetics of pore formation. Fig. 23 indicates that when values of k_{a1} are used, which characterize the pore formation process at earlier times (5-10 min), the experimental data for BaxC-KK agree with $n \approx$ 3-4 for POPC membranes (Fig. 23*A*) and $n \approx$ 2-3 for POPC/POPG membranes (Fig. 23*B*). When values of k_{a2} are used, which characterize further progression of pore formation process, the data are consistent with $n \approx 8$ for POPC membranes (Fig. 23*C*) and $n \approx 5$ for POPC/POPG membranes (Fig. 23*D*). Thus, the overall picture of membrane pore formation by the wild-type BaxC-KK peptide is that the peptide molecules form an initial nucleation complex involving 2-4 molecules and characterized with affinity constants of $(1.3\text{-}3.7)\times10^{6}$ M^{-1} followed by a more efficient process (higher 2^{nd} order rate constant) of the assembly of the final pore structure involving up to 8 peptide molecules associated with affinity constants of $(0.5\text{-}1.4)\times10^{7}$ M^{-1}.

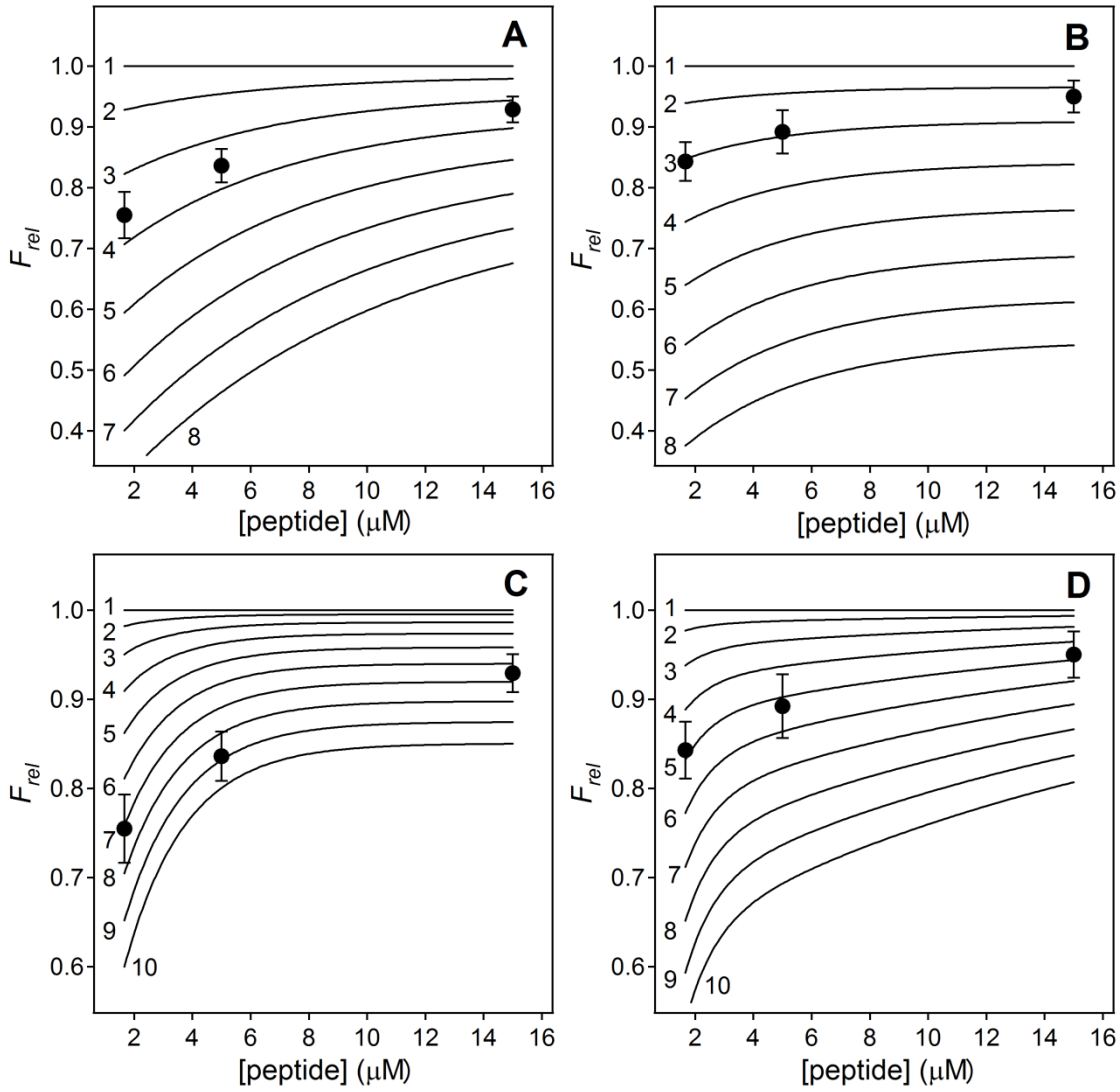

Figure 23: Figure indicates that when values of k_{a1} are used, which characterize the pore formation process at earlier times (5-10 min), the experimental data for BaxC-KK agree with n~ 3-4 for POPC membranes (A) and n ~ 2-3 for POPC/POPG membranes (B). When values of k_{a2} are used, which characterize further progression of pore formation process, the data are consistent with n~ 8 for POPC membranes (C) and n~5 for POPC/POPG membranes (D).

Depth of membrane insertion was performed to determine the varying rupturing power of different petides in two different lipid compositions. These studies were performed to complement our understanding of how these peptides create pores in the membranes and how much they differ from each other in their pore forming abilities. Using brominated lipids, the position of tryptophan is determined and it is seen that for pure POPC membranes, Trp16 sits at a farther distance from the membrane center, both above and below while it got inserted much deeper when the lipid was incorporated with 30% POPG. Additionally with 30% POPG composition, the insertion ability differs with each mutant and Bax KK was seen to have the highest penetration into the membrane while Bax LL showed the least. This is in contrast with the pure POPC membranes where all three mutants share almost similar insertion. From all these studies, we conclude that wild type Bax has the highest penetration in the lipid membrane and would expedite the release of cytochrome c.

We have seen that Bax peptide and its mutants penetrate into the lipid membrane and have a certain depth of insertion; we are interested in determining the secondary structures for the peptide in various environments. As the peptide is exposed more to the buffer, the amount of β sheets increase while α helices go down. In the dry sample, more α-helices are seen and in the hydrated sample, amount of β−sheets increases dramatically. This indicates that the mode of action of Bax C-terminal peptide may involve a β barrel-like structure. In conclusion, our studies have identified that Bax C-terminal peptide itself has the potency of forming relatively large pores in lipid membranes. The wild type peptide with two lysine residues is more potent than the charge-reversal or charge neutralization mutant peptides in pore formation. CD and FTIR studies indicate that under physiologically relevant conditions, the peptide's secondary structure

contains significant fractions of β-sheet. Finally, fluorescence quenching experiments identify a pattern of membrane insertion of the peptides that is consistent with a β-barrel-type structure of membrane pores. It should be expected that the behavior of the isolated peptides would be different than when it is attached to the protein. However, these findings are encouraging in terms of developing cytotoxic peptide-based molecular tools for cell membrane perforation and killing of unwanted cells such as bacteria, fungi, or cancer cells.

REFERENCES

Annis, M. G., Soucie, E. L., Dlugosz, P. J., Cruz-Aguado, J. A., Penn, L. Z., Leber, B., & Andrews, D. W. (2005). Bax forms multispanning monomers that oligomerize to permeabilize membranes during apoptosis. *The EMBO Journal, 24*(12), 2096-2103.

Ashkenazi, A. (2002). Targeting death and decoy receptors of the tumour-necrosis factor superfamily. *Nature Reviews Cancer, 2*(6), 420-430.

Ausili, A., Torrecillas, A., Martínez-Senac, M. M., Corbalán-García, S., & Gómez-Fernández, J. C. (2008). The interaction of the bax C-terminal domain with negatively charged lipids modifies the secondary structure and changes its way of insertion into membranes. *Journal of Structural Biology, 164*(1), 146-152.

Bensikaddour, H., Fa, N., Burton, I., Deleu, M., Lins, L., Schanck, A., . . . Mingeot-Leclercq, M. P. (2008). Characterization of the interactions between fluoroquinolone antibiotics and lipids: A multitechnique approach. *Biophysical Journal, 94*(8), 3035-3046.

Brenner, C., Cadiou, H., Vieira, H. L. A., Zamzami, N., Marzo, I., Xie, Z., . . . Reed, J. C. (2000). Bcl-2 and bax regulate the channel activity of the mitochondrial adenine nucleotide translocator. *Oncogene, 19*(3), 329-336.

Brunet, A., Bonni, A., Zigmond, M. J., Lin, M. Z., Juo, P., Hu, L. S., . . . Greenberg, M. E. (1999). Akt promotes cell survival by phosphorylating and inhibiting a forkhead transcription factor. *Cell, 96*(6), 857-868.

Brustovetsky, T., Antonsson, B., Jemmerson, R., Dubinsky, J. M., & Brustovetsky, N. (2005). Activation of calcium - independent phospholipase A2 (iPLA2) in brain mitochondria and release of apoptogenic factors by BAX and truncated BID. *Journal of Neurochemistry, 94*(4), 980-994.

Brustovetsky, T., Li, T., Yang, Y., Zhang, J. T., Antonsson, B., & Brustovetsky, N. (2010). BAX insertion, oligomerization, and outer membrane permeabilization in brain mitochondria: Role of permeability transition and SH-redox regulation. *Biochimica Et Biophysica Acta (BBA)-Bioenergetics,*

Ceru, S., Jenko-Kokalj, S., Rabzelj, S., Škarabot, M., Gutierrez-Aguirre, I., Kopitar-Jerala, N., . . . Zerovnik, E. (2008). Size and morphology of toxic oligomers of amyloidogenic proteins: A case study of human stefin B. *Amyloid, 15*(3), 147-159.

Chen, Y. H., Yang, J. T., & Martinez, H. M. (1972). Determination of the secondary structures of proteins by circular dichroism and optical rotatory dispersion. *Biochemistry, 11*(22), 4120-4131.

Choo, L. P., Wetzel, D. L., Halliday, W. C., Jackson, M., LeVine, S. M., & Mantsch, H. H. (1996). In situ characterization of beta-amyloid in alzheimer's diseased tissue by synchrotron fourier transform infrared microspectroscopy. *Biophysical Journal, 71*(4), 1672-1679.

del Mar Martínez-Senac, M., Corbalán-García, S., & Gómez-Fernández, J. C. (2001). Conformation of the C-terminal domain of the pro-apoptotic protein bax and mutants and its interaction with membranes. *Biochemistry, 40*(33), 9983-9992.

Dillner, U. (1994). Thermal modeling of multilayer membranes for sensor applications. *Sensors and Actuators A: Physical, 41*(1-3), 260-267.

Fa, N., Ronkart, S., Schanck, A., Deleu, M., Gaigneaux, A., Goormaghtigh, E., & Mingeot-Leclercq, M. P. (2006). Effect of the antibiotic azithromycin on thermotropic behavior of DOPC or DPPC bilayers. *Chemistry and Physics of Lipids, 144*(1), 108-116.

Frey, S., & Tamm, L. K. (1991). Orientation of melittin in phospholipid bilayers. A polarized attenuated total reflection infrared study. *Biophysical Journal, 60*(4), 922-930.

Fu, F. N., Lomneth, R. B., Cai, S., & Singh, B. R. (1998). Role of zinc in the structure and toxic activity of botulinum neurotoxin. *Biochemistry, 37*(15), 5267-5278.

Fu, F. N., & Singh, B. R. (1999). Calcein permeability of liposomes mediated by type A botulinum neurotoxin and its light and heavy chains. *Journal of Protein Chemistry, 18*(6), 701-707.

Garcia-Saez, A. J., Fuertes, G., Suckale, J., & Salgado, J. (2010). Permeabilization of the outer mitochondrial membrane by Bcl-2 proteins. *Advances in Experimental Medicine and Biology, 677*, 91-105.

Gogvadze, V., Orrenius, S., & Zhivotovsky, B. (2006). Multiple pathways of cytochrome c release from mitochondria in apoptosis. *Biochimica Et Biophysica Acta (BBA)-Bioenergetics, 1757*(5-6), 639-647.

Goormaghtigh, E., Cabiaux, V., & RUYSSCHAERT, J. M. (1990). Secondary structure and dosage of soluble and membrane proteins by attenuated total reflection Fourier - transform

infrared spectroscopy on hydrated films. *European Journal of Biochemistry, 193*(2), 409-420.

Ivanov, D., Dubreuil, N., Raussens, V., Ruysschaert, J. M., & Goormaghtigh, E. (2004). Evaluation of the ordering of membranes in multilayer stacks built on an ATR-FTIR germanium crystal with atomic force microscopy: The case of the H , K -ATPase-containing gastric tubulovesicle membranes. *Biophysical Journal, 87*(2), 1307-1315.

Jackson, M., Haris, P. I., & Chapman, D. (1989). Conformational transitions in poly (-lysine): Studies using fourier transform infrared spectroscopy. *Biochimica Et Biophysica Acta (BBA)-Protein Structure and Molecular Enzymology, 998*(1), 75-79.

Jackson, M., & Mantsch, H. H. (1995). The use and misuse of FTIR spectroscopy in the determination of protein structure. *Critical Reviews in Biochemistry and Molecular Biology, 30*(2), 95-120.

Karbowski, M., & Youle, R. (2003). Dynamics of mitochondrial morphology in healthy cells and during apoptosis. *Cell Death & Differentiation, 10*(8), 870-880.

Kaushik, S., Krishnan, A., Prausnitz, M. R., & Ludovice, P. J. (2001). Magainin-mediated disruption of stratum corneum lipid vesicles. *Pharmaceutical Research, 18*(6), 894-896.

Kim, Y. C., Ludovice, P. J., & Prausnitz, M. R. (2007). Transdermal delivery enhanced by magainin pore-forming peptide. *Journal of Controlled Release, 122*(3), 375-383.

Klocek, G., Schulthess, T., Shai, Y., & Seelig, J. (2009). Thermodynamics of melittin binding to lipid bilayers. aggregation and pore formation†. *Biochemistry, 48*(12), 2586-2596.

Kuwana, T., Mackey, M. R., Perkins, G., Ellisman, M. H., Latterich, M., Schneiter, R., . . . Newmeyer, D. D. (2002). Bid, bax, and lipids cooperate to form supramolecular openings in the outer mitochondrial membrane. *Cell, 111*(3), 331-342.

Liu, Y., & Regen, S. L. (1993). Control over vesicle rupture and leakage by membrane packing and by the aggregation state of an attacking surfactant. *Journal of the American Chemical Society, 115*(2), 708-713.

Lovell, J. F., Billen, L. P., Bindner, S., Shamas-Din, A., Fradin, C., Leber, B., & Andrews, D. W. (2008). Membrane binding by tBid initiates an ordered series of events culminating in membrane permeabilization by bax. *Cell, 135*(6), 1074-1084.

Mancinelli, F., Caraglia, M., Budillon, A., Abbruzzese, A., & Bismuto, E. (2006). Molecular dynamics simulation and automated docking of the pro - apoptotic bax protein and its complex with a peptide designed from the Bax - binding domain of anti - apoptotic Ku70. *Journal of Cellular Biochemistry, 99*(1), 305-318.

Marsh, D. (1999). Quantitation of secondary structure in ATR infrared spectroscopy. *Biophysical Journal, 77*(5), 2630-2637.

Martínez-Senac, M. M., Corbalán-García, S., & Gómez-Fernández, J. C. (2002). The structure of the C-terminal domain of the pro-apoptotic protein bak and its interaction with model membranes. *Biophysical Journal, 82*(1), 233-243.

Matsuzaki, K., Murase, O., Fujii, N., & Miyajima, K. (1995). Translocation of a channel-forming antimicrobial peptide, magainin 2, across lipid bilayers by forming a pore. *Biochemistry, 34*(19), 6521-6526.

Nieva, J. L., Agirre, A., Nir, S., & Carrasco, L. (2003). Mechanisms of membrane permeabilization by picornavirus 2B viroporin. *FEBS Letters, 552*(1), 68-73.

Nir, S., & Nieva, J. L. (2000). Interactions of peptides with liposomes: Pore formation and fusion. *Progress in Lipid Research, 39*(2), 181-206.

Ochoa, W. F., Garcia-Garcia, J., Fita, I., Corbalan-Garcia, S., Verdaguer, N., & Gomez-Fernandez, J. C. (2001). Structure of the C2 domain from novel protein kinase C. A membrane binding model for Ca2 -independent C2 domains1. *Journal of Molecular Biology, 311*(4), 837-849.

Oh, J. H., Park, H. H., Do, K. Y., Han, M., Hyun, D. H., Kim, C. G., . . . Shin, S. C. (2008). Influence of the delivery systems using a microneedle array on the permeation of a hydrophilic molecule, calcein. *European Journal of Pharmaceutics and Biopharmaceutics, 69*(3), 1040-1045.

Ott, M., Norberg, E., Zhivotovsky, B., & Orrenius, S. (2009). Mitochondrial targeting of tBid/Bax: A role for the TOM complex&quest. *Cell Death & Differentiation, 16*(8), 1075-1082.

Pande, A. H., Qin, S., Nemec, K. N., He, X., & Tatulian, S. A. (2006). Isoform-specific membrane insertion of secretory phospholipase A2 and functional implications. *Biochemistry, 45*(41), 12436-12447.

Parente, R. A., Nir, S., & Szoka Jr, F. C. (1990). Mechanism of leakage of phospholipid vesicle contents induced by the peptide GALA. *Biochemistry, 29*(37), 8720-8728.

Park, J. H., Allen, M. G., & Prausnitz, M. R. (2006). Polymer microneedles for controlled-release drug delivery. *Pharmaceutical Research, 23*(5), 1008-1019.

Petros, A. M., Olejniczak, E. T., & Fesik, S. W. (2004). Structural biology of the bcl-2 family of proteins. *Biochimica Et Biophysica Acta (BBA)-Molecular Cell Research, 1644*(2-3), 83-94.

Qin, S., Pande, A. H., Nemec, K. N., & Tatulian, S. A. (2004). The N-terminal [alpha]-helix of pancreatic phospholipase A2 determines productive-mode orientation of the enzyme at the membrane surface. *Journal of Molecular Biology, 344*(1), 71-89.

Rabzelj, S., Viero, G., Gutiérrez - Aguirre, I., Turk, V., Dalla Serra, M., Anderluh, G., & Žerovnik, E. (2008). Interaction with model membranes and pore formation by human stefin B–studying the native and prefibrillar states. *FEBS Journal, 275*(10), 2455-2466.

Rapaport, D., Peled, R., Nir, S., & Shai, Y. (1996). Reversible surface aggregation in pore formation by pardaxin. *Biophysical Journal, 70*(6), 2502-2512.

Raussens, V., Narayanaswami, V., Goormaghtigh, E., Ryan, R. O., & Ruysschaert, J. M. (1996). Hydrogen/deuterium exchange kinetics of apolipophorin-III in lipid-free and phospholipid-bound states. *Journal of Biological Chemistry, 271*(38), 23089.

Ray, S., Scott, J. L., & Tatulian, S. A. (2007). Effects of lipid phase transition and membrane surface charge on the interfacial activation of phospholipase A2. *Biochemistry, 46*(45), 13089-13100.

Reed, J. (2006). Proapoptotic multidomain bcl-2/Bax-family proteins: Mechanisms, physiological roles, and therapeutic opportunities. *Cell Death & Differentiation, 13*(8), 1378-1386.

Rodionova, N. A., Tatulian, S. A., Surrey, T., Jaehnig, F., & Tamm, L. K. (1995). Characterization of two membrane-bound forms of OmpA. *Biochemistry, 34*(6), 1921-1929.

Seelig, J., Nebel, S., Ganz, P., & Bruns, C. (1993). Electrostatic and nonpolar peptide-membrane interactions. lipid binding and functional properties of somatostatin analogs of charge z= 1 to z= 3. *Biochemistry, 32*(37), 9714-9721.

Surewicz, W. K., Mantsch, H. H., & Chapman, D. (1993). Determination of protein secondary structure by fourier transform infrared spectroscopy: A critical assessment. *Biochemistry, 32*(2), 389-394.

Suzuki, M., Youle, R. J., & Tjandra, N. (2000). Structure of bax:: Coregulation of dimer formation and intracellular localization. *Cell, 103*(4), 645-654.

Tamm, L. K., & Tatulian, S. A. (1993). Orientation of functional and nonfunctional PTS permease signal sequences in lipid bilayers. A polarized attenuated total reflection infrared study. *Biochemistry, 32*(30), 7720-7726.

Tamm, L. K., & Tatulian, S. A. (1997). Infrared spectroscopy of proteins and peptides in lipid bilayers. *Quarterly Reviews of Biophysics, 30*(04), 365-429.

Tatulian, S. A. (2003). Attenuated total reflection fourier transform infrared spectroscopy: A method of choice for studying membrane proteins and lipids. *Biochemistry, 42*(41), 11898-11907.

Tatulian, S. A., Cortes, D. M., & Perozo, E. (1998). Structural dynamics of the streptomyces lividans K channel (SKC1): Secondary structure characterization from FTIR spectroscopy. *FEBS Letters, 423*(2), 205-212.

Tatulian, S. A., Jones, L. R., Reddy, L. G., Stokes, D. L., & Tamm, L. K. (1995). Secondary structure and orientation of phospholamban reconstituted in supported bilayers from polarized attenuated total reflection FTIR spectroscopy. *Biochemistry, 34*(13), 4448-4456.

Tatulian, S. A., Qin, S., Pande, A. H., & He, X. (2005). Positioning membrane proteins by novel protein engineering and biophysical approaches. *Journal of Molecular Biology, 351*(5), 939-947.

Tatulian, S. A., & Tamm, L. K. (2000). Secondary structure, orientation, oligomerization, and lipid interactions of the transmembrane domain of influenza hemagglutinin. *Biochemistry, 39*(3), 496-507.

Tatulian, S., Hinterdorfer, P., Baber, G., & Tamm, L. (1995). Influenza hemagglutinin assumes a tilted conformation during membrane fusion as determined by attenuated total reflection FTIR spectroscopy. *The EMBO Journal, 14*(22), 5514.

Torrecillas, A., Corbalán-García, S., & Gómez-Fernández, J. C. (2004). An infrared spectroscopic study of the secondary structure of protein kinase Cα and its thermal denaturation. *Biochemistry, 43*(8), 2332-2344.

Torrecillas, A., Martínez-Senac, M. M., Ausili, A., Corbalán-García, S., & Gómez-Fernández, J. C. (2007). Interaction of the C-terminal domain of bcl-2 family proteins with model membranes. *Biochimica Et Biophysica Acta (BBA)-Biomembranes, 1768*(11), 2931-2939.

Torrecillas, A., Martínez-Senac, M. M., Goormaghtigh, E., de Godos, A., Corbalán-García, S., & Gómez-Fernández, J. C. (2005). Modulation of the membrane orientation and secondary structure of the C-terminal domains of bak and bcl-2 by lipids. *Biochemistry, 44*(32), 10796-10809.

Tschammer, N. (2007). *Helical Packing Regulates Structural Transitions in BAX,*

van de Weert, M., Haris, P. I., Hennink, W. E., & Crommelin, D. J. A. (2001). Fourier transform infrared spectrometric analysis of protein conformation: Effect of sampling method and stress factors. *Analytical Biochemistry, 297*(2), 160-169.

Van't Hof, R., Van Klompenburg, W., Pilon, M., Kozubek, A., de Korte-Kool, G., Demel, R., . . . De Kruijff, B. (1993). The transit sequence mediates the specific interaction of the precursor of ferredoxin with chloroplast envelope membrane lipids. *Journal of Biological Chemistry, 268*(6), 4037.

Veresov, V. G., & Davidovskii, A. I. (2009). Activation of bax by joint action of tBid and mitochondrial outer membrane: Monte carlo simulations. *European Biophysics Journal, 38*(7), 941-960.

Vigano, C., Smeyers, M., Raussens, V., Scheirlinckx, F., Ruysschaert, J., & Goormaghtigh, E. (2004). Hydrogen - deuterium exchange in membrane proteins monitored by IR

spectroscopy: A new tool to resolve protein structure and dynamics. *Biopolymers, 74*(1 - 2), 19-26.

Vogel, M., Münster, C., Fenzl, W., & Salditt, T. (2000). Thermal unbinding of highly oriented phospholipid membranes. *Physical Review Letters, 84*(2), 390-393.

Willis, S. N., Chen, L., Dewson, G., Wei, A., Naik, E., Fletcher, J. I., . . . Huang, D. (2005). Proapoptotic bak is sequestered by mcl-1 and bcl-xL, but not bcl-2, until displaced by BH3-only proteins. *Genes & Development, 19*(11), 1294.

Winkowski, K., Ludescher, R. D., & Montville, T. J. (1996). Physiochemical characterization of the nisin-membrane interaction with liposomes derived from listeria monocytogenes. *Applied and Environmental Microbiology, 62*(2), 323.

Yip, K., & Reed, J. (2008). Bcl-2 family proteins and cancer. *Oncogene, 27*(50), 6398-6406.

Yu, J., & Zhang, L. (2004). Apoptosis in human cancer cells. *Current Opinion in Oncology, 16*(1), 19.

Zeth, K. (2010). Structure and evolution of mitochondrial outer membrane proteins of [beta]-barrel topology. *Biochimica Et Biophysica Acta (BBA)-Bioenergetics, 1797*(6-7), 1292-1299.

Zhai, L., Zhao, J., Zhao, M., Chen, Y., & Zhang, L. (2007). Encapsulation and releasing of calcein by spontaneously formed zwitterionic/anionic vesicle without separation. *Journal of Dispersion Science and Technology, 28*(3), 455-461.

Zong, W. X., Li, C., Hatzivassiliou, G., Lindsten, T., Yu, Q. C., Yuan, J., & Thompson, C. B. (2003). Bax and bak can localize to the endoplasmic reticulum to initiate apoptosis. *The Journal of Cell Biology, 162*(1), 59.